Article

SOURCE DATA | TRANSPARENT PROCESS

EMBO reports

Nuclear envelope rupture and NET formation is driven by PKCα-mediated lamin B disassembly

Yubin Li[1,2], Minghui Li[1,2,3], Bettina Weigel[4,5,6], Moritz Mall[4,5,6], Victoria P Werth[1,2] & Ming-Lin Liu[1,2,*]

Abstract

The nuclear lamina is essential for the structural integration of the nuclear envelope. Nuclear envelope rupture and chromatin externalization is a hallmark of the formation of neutrophil extracellular traps (NETs). NET release was described as a cellular lysis process; however, this notion has been questioned recently. Here, we report that during NET formation, nuclear lamin B is not fragmented by destructive proteolysis, but rather disassembled into intact full-length molecules. Furthermore, we demonstrate that nuclear translocation of PKCα, which serves as the kinase to induce lamin B phosphorylation and disassembly, results in nuclear envelope rupture. Decreasing lamin B phosphorylation by PKCα inhibition, genetic deletion, or by mutating the PKCα consensus sites on lamin B attenuates extracellular trap formation. In addition, strengthening the nuclear envelope by lamin B overexpression attenuates NET release *in vivo* and reduces levels of NET-associated inflammatory cytokines in UVB-irradiated skin of lamin B transgenic mice. Our findings advance the mechanistic understanding of NET formation by showing that PKCα-mediated lamin B phosphorylation drives nuclear envelope rupture for chromatin release in neutrophils.

Keywords lamin B disassembly; NET formation; nuclear envelope rupture; PKCα

Subject Categories Cell Adhesion, Polarity & Cytoskeleton; Immunology; Signal Transduction

DOI 10.15252/embr.201948779 | Received 1 July 2019 | Revised 22 May 2020 | Accepted 25 May 2020 | Published online 15 June 2020

EMBO Reports (2020) 21: e48779

Introduction

Neutrophils are the most common leukocytes. Increasing evidence from many studies (Brinkmann *et al*, 2004; Lood *et al*, 2016; Soehnlein *et al*, 2017; Boeltz *et al*, 2019), including our own (Folkesson *et al*, 2015), indicates the importance of neutrophils in acute or chronic inflammation in variety of human diseases (Brinkmann *et al*, 2004; Lood *et al*, 2016; Soehnlein *et al*, 2017; Boeltz *et al*, 2019). NET formation is characterized by nuclear chromatin decondensation (Brinkmann *et al*, 2004) through peptidyl arginine deiminase type IV (PAD4)-catalyzed histone citrullination (Neeli *et al*, 2008; Wang *et al*, 2009) or neutrophil elastase-mediated histone cleavage (Pieterse *et al*, 2018), followed by chromatin extrusion via the ruptured nuclear envelope. The externalized nuclear chromatin serves as the backbone of NETs that mix with cytosolic contents, i.e., granule proteins and oxidized mitochondrial DNA, and form the extracellular trap structure (Boeltz *et al*, 2019). Several signaling pathways may be important in the development of NET formation, i.e., production of reactive oxygen species (ROS) through NADPH oxidase (NOX2)-dependent or NADPH oxidase (NOX2)-independent pathways (Douda *et al*, 2015; Pieterse *et al*, 2018; Boeltz *et al*, 2019), activation of protein kinase C (PKC), extracellular-signal-regulated kinase (ERK/MAPK), and phosphatidylinositide 3-kinase (PI3K)/Akt (Boeltz *et al*, 2019).

ROS is thought to be required for the release of myeloperoxidase and neutrophil elastase from granules in activated neutrophils. Then, neutrophil elastase is translocated to the nucleus for chromatin decondensation by histone cleavage in the early stage of NET formation (Fuchs *et al*, 2007; Papayannopoulos *et al*, 2010). However, a very recent consensus statement paper by experts in the field suggests that the direct connection between lysosomal membrane instability and NET formation is still under discussion (Boeltz *et al*, 2019). Pieterse *et al* (2018) reported that neutrophil elastase may be associated with cleavage of the N-terminal tail, the proteolytic sensitive region, of histones in the late stage of NET formation. Another paper reported that neutrophils from neutrophil elastase-deficient mice could still undergo NET formation (Martinod *et al*, 2016). In addition to ROS-dependent NET formation, a number of recent studies also reported ROS-independent NET formation induced by certain stimuli (Rochael *et al*, 2015; Tatsiy & McDonald, 2018).

Nuclear envelope rupture is the hallmark and a prerequisite step in the multi-step process of NET formation (Boeltz *et al*, 2019). However, the relevant cellular and molecular mechanism of nuclear envelope rupture during NET formation is still unclear. NET formation was described as a lytic cell death mechanism (Fuchs *et al*,

1 Corporal Michael J. Crescenz VAMC, Philadelphia, PA, USA
2 Department of Dermatology, Perelman School of Medicine, University of Pennsylvania, Philadelphia, PA, USA
3 Department of Rheumatology and Immunology, Tianjin Medical University General Hospital, Tianjin, China
4 Cell Fate Engineering and Disease Modeling Group, German Cancer Research Center (DKFZ) and DKFZ-ZMBH Alliance, Heidelberg, Germany
5 HITBR Hector Institute for Translational Brain Research GmbH, Heidelberg, Germany
6 Central Institute of Mental Health, Medical Faculty Mannheim, Heidelberg University, Mannheim, Germany
*Corresponding author. Tel: +1 215 614 1621; E-mail: lium1@pennmedicine.upenn.edu

2007; Papayannopoulos *et al*, 2010; Yipp & Kubes, 2013). However, this notion has been questioned by several recent observations (Amulic *et al*, 2017; Neubert *et al*, 2018). Rupture of the nuclear envelope appears to be a distinct process from previously described lysis or dissolution of the nuclear envelope (Amulic *et al*, 2017; Neubert *et al*, 2018). In addition, Pilsczek *et al* (2010) described vital, but not lytic, NET formation in which NETs are released via nuclear budding or vesicle release by an unknown mechanism.

The nuclear envelope consists of outer and inner lipid nuclear membranes (ONM and INM) and nuclear lamina, a protein filament meshwork that provides structural scaffold to reinforce nuclear envelope integrity (Goldberg *et al*, 2008). Nuclear lamins are categorized as either A-type (A, C) or B-type (B_1, B_2) lamins (Goldberg *et al*, 2008). A-type lamins form thick filament bundles that contribute to the mechanical stiffness of nuclei (Lammerding *et al*, 2006; Goldberg *et al*, 2008; Rowat *et al*, 2013), whereas B-type lamins form thin but highly organized meshworks that are crucial to the integrity and elasticity of the nuclear envelope (Vergnes *et al*, 2004; Goldberg *et al*, 2008), but not stiffness (Lammerding *et al*, 2006; Swift *et al*, 2013). Shin *et al* reported that nuclear stiffness increases with the lamin A:B ratio (Shin *et al*, 2013), and increasing the lamin A:B ratio by downregulation of lamin B promotes nuclear stiffness in hematopoietic cells (Shin *et al*, 2013). Lamin B is anchored underneath the INM through the lamin B receptor (LBR) (Olins *et al*, 2008; Singh *et al*, 2016). Nuclear envelope breakdown (Hatch & Hetzer, 2014) is a common cellular event in nuclear fragmentation during cell apoptosis (Shimizu *et al*, 1998), in nuclear division during cell mitosis (Collas *et al*, 1997; Mall *et al*, 2012), and in viral nuclear access during viral infection (Park & Baines, 2006). In the cellular processes described above, nuclear lamin B is either proteolytically degraded by caspases (Slee *et al*, 2001) or disassembled through phosphorylation by protein kinase C (PKC) (Collas *et al*, 1997; Muranyi *et al*, 2002).

Mature neutrophils are terminally differentiated cells thought to have an unusual nucleus with a paucity of lamin A/C (Olins *et al*, 2008) and a reduced amount of lamin B (Olins *et al*, 2008). Recent studies, however, reported that neutrophils do have A-type (Amulic *et al*, 2017) and B-type (Moisan & Girard, 2006; Rowat *et al*, 2013) lamins. The role of lamin B in neutrophil biology is unclear and was ignored, and the involvement of lamin B in NET formation has not been investigated. In the current study, we investigated the importance of lamin B for the integrity of the nucleus in neutrophils and cellular mechanisms that regulate nuclear envelope rupture during NET formation in neutrophils from human and mice. We also investigated the effect of strengthening the nuclear envelope by lamin B overexpression on NET formation *in vivo* and on the presence of NET-associated inflammatory cytokines in UVB-irradiated skin of lamin B transgenic mice.

Results

Nuclear lamin B is a substantial component of the nuclear envelope that is involved in NET formation

Neutrophils are terminally differentiated cells, and the role of nuclear lamina in neutrophil biology is not well understood (Olins *et al*, 2008). However, nuclear envelope breakdown is required for nuclear chromatin externalization during NET formation. To explore the role of nuclear lamin B, we detected the expression of lamin B in primary human polymorphonuclear neutrophils (pPMNs) and the involvement of lamin B in NET formation (Fig 1A and B). NET formation can be triggered by PMA, the most commonly used NET inducer (Fig 1A; Brinkmann *et al*, 2004), or by platelet activating factor (PAF), a UVB-induced lipid mediator and naturally existing stimulus of NETs (Damiani & Ullrich, 2016). Confocal microscopy analyses indicated that

Figure 1. Nuclear lamin B is a substantial component of nuclear envelope that is involved in NET formation.

A Summary and representative analysis of NET formation of pPMNs stimulated by 50 nM PMA for 3 h, detected by fluorescent microplate reader and confocal microscopy, respectively. Scale bar 20 μm.

B Representative confocal microscopy images of pPMNs that were treated without (control) or with 50 nM PMA for 3 h and stained for lamin B and DNA as described in panel (B). The light blue arrows indicate the release of decondensed DNA associated with lamin B molecules from ruptured nuclear envelope. Scale bar 10 μm.

C Schematic cross-section of a cell and portion of the nucleus and the nuclear envelope, as well as the ones with corresponding overexpression of lamin B. The two lipid bilayers of the nuclear envelope are the inner and outer nuclear membranes (INM and ONM, respectively). The meshwork, nuclear lamin B is anchored to INM through lamin B receptor (LBR).

D Representative and summary of immunoblots of lamin B of bone marrow neutrophils from WT and $Lmnb1^{TG}$ mice. Vinculin served as loading control.

E Summary analysis of PAF-induced NET formation in mPMNs from WT vs. $Lmnb1^{TG}$ mice that were stimulated without or with 10 μM PAF for 3 h and then fixed by 2% PFA and stained by SYTOX Green, followed by detection with fluorescent microplate reader.

F The endpoint analysis of NET-DNA release index was detected by coincubation of primary mouse peritoneal mPMNs from WT and $Lmnb1^{TG}$ mice without (control) or with 10 μM PAF in medium containing 1 μM SYTOX Green dye with recording by a microplate reader at the 3-h time point. The NET-DNA release index was reported in comparison with an assigned value of 100% for the total DNA released by neutrophils lysed by 0.5% (*v/v*) Triton X-100.

G, H Representative images (G) and summary analysis (H) of PAF-induced NET formation in mPMNs from WT vs. $Lmnb1^{TG}$ mice that were stimulated without or with 10 μM PAF for 3 h and stained with both cell-permeable SYTO Red and cell-impermeable SYTOX Green, without fixation. Images were taken by Olympus confocal microscopy, followed by automated quantification of NETs on 5–6 non-overlapping area per well using ImageJ for calculation of % cells with NET formation. (G) Scale bars, 40 μm.

Data information: Panels (A, D, E, F, H) were summary analysis of NET formation (A, E), or summary analyses of immunoblots (D), DNA% release index (F) that were calculated based on the arbitrary fluorescent readout unit (A, E), immunoblot arbitrary unit (D). NET-DNA release index calculated based on fluorescent readout (F), or % cells with NET formation by image analysis (H). Data in (A, D, E, F, H) represent mean ± SD (n = 3–5 biological replicates). *$P < 0.05$, **$P < 0.01$, ***$P < 0.001$ between groups as indicated. Comparisons among three or more groups were performed using ANOVA, followed by Student–Newman–Keuls test. Comparison between two groups was analyzed by the Student t test.
Source data are available online for this figure.

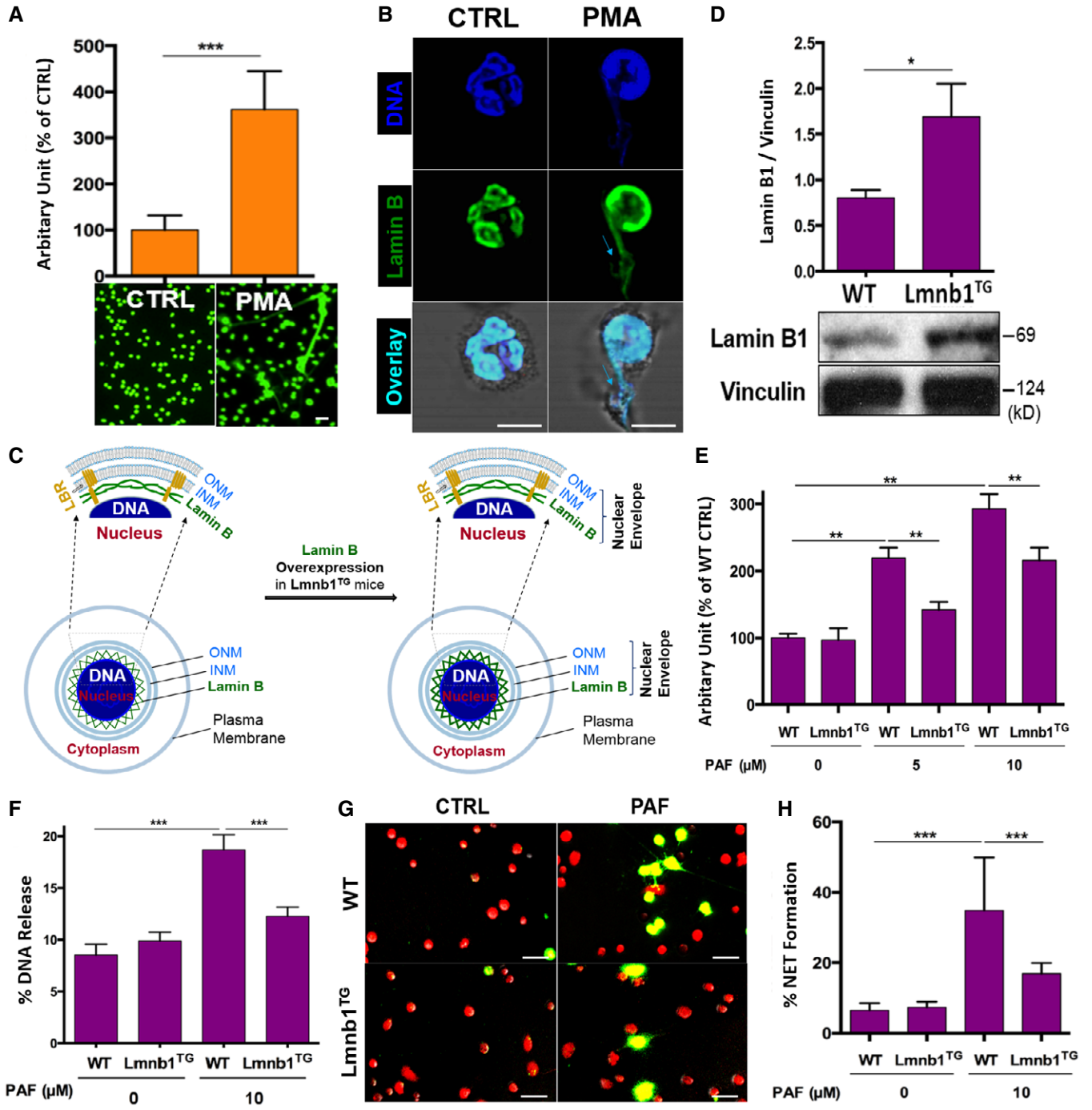

Figure 1.

nuclear lamin B is a substantial component of the nuclear envelope (Fig 1B and C), which is ruptured during NET release (Fig 1B), indicating the involvement of lamin B in the process of NET formation.

Lamin B is assembled as a filament meshwork that lies beneath the INM, and the two are associated by an integral protein, lamin B receptor (Fig 1C). Given the importance of lamin B in nuclear envelope integration (Vergnes *et al*, 2004; Goldberg *et al*, 2008), one may propose that lamin B may be important in regulating nuclear envelope rupture during NET formation. To test this hypothesis, we first explored the effects of lamin B overexpression on NET formation by using neutrophils from lamin B transgenic Lmnb1^{TG} mice (Fig 1D). We found attenuated NET formation in peritoneal neutrophils from Lmnb1^{TG} mice as compared to those from their WT littermates (Fig 1E–H), analyzed by fluorometric NET quantification (Fig 1E; Sollberger *et al*, 2016), endpoint analysis of NET-DNA release index (Fig 1F; Douda *et al*, 2015; Khan *et al*, 2018), and immunofluorescent imaging analysis of NET formation (Fig 1G and H; Sollberger *et al*, 2016). On the other hand,

lamin B maturation is regulated by farnesylation (Adam *et al*, 2013), and long-term inhibition of protein farnesylation with farnesyltransferase inhibitor (FTI) can reduce the amount of mature lamin B (Adam *et al*, 2013). To explore the effects of decreased lamin B, we found that coincubation with FTI can reduce the amount of mature lamin B both in differentiated HL-60 neutrophils (dPMNs) (Fig EV1A) and in RAW 264.7 macrophages (Fig EV1C). Most importantly, we found that decreased lamin B in FTI-pretreated cells could enhance PAF-induced extracellular trap formation both in dPMNs and in RAW264.7 cells (Fig EV1B, D and E). Taken together, the levels of mature lamin B expression in the nucleus affected extracellular trap formation in a negative dose-dependent manner both in neutrophils and macrophages.

Therefore, our results demonstrated that nuclear lamin B is a substantial component of the nuclear envelope in neutrophils, similar to other cell types (Vergnes *et al*, 2004; Goldberg *et al*, 2008). Nuclear lamin B is important in regulating nuclear envelop breakdown and release of extracellular traps.

Nuclear lamin B disassembly, but not proteolytic cleavage, is responsible for nuclear envelope rupture during NET formation

Next, we sought to elucidate how lamin B is involved in nuclear envelope rupture during NET formation. Unexpectedly, immunoblot analysis of the time-course studies demonstrated that nuclear lamin B remained as an intact full-length molecule during NET formation in human dPMNs 0–3 h after stimulation by PMA (Fig 2A and B) or PAF (Fig 2C and D), in contrast to the destructively cleaved and fragmented lamin B in apoptotic neutrophils (Fig 2A). Importantly, immunoblot analysis of isolated extracellular NETs (Fig 2E) showed that nuclear lamin B is also released with NETs to the extracellular space and NET-associated lamin B was not degraded, but remained as an intact full-length molecule (Fig 2E), confirming the findings from the whole-cell lysates. In contrast to uncleaved nuclear lamin B, we observed cleaved histone H3 in the neutrophils with NET formation (Fig 2E). Neutrophil elastase may contribute to the cleavage of histone H3 and decondensation of chromatin during NET formation (Konig & Andrade, 2016; Pieterse *et al*, 2018). Therefore, our results suggested potential disassembly, but not the destructive cleavage, of lamin B is responsible for nuclear envelope rupture and extracellular trap formation during NET formation in neutrophils.

Caspase-3 mediates apoptosis and cleaves lamin B (Slee *et al*, 2001) during apoptotic nuclear fragmentation. In the current study, we found that caspase-3 remained inactive as pro-caspase-3 over a 3-h period of time during NET formation (Fig 2F), while activated caspase-3 was detected in apoptotic dPMNs induced by extended PMA treatment (Arroyo *et al*, 2002) for 12–24 h (Fig 2G). Furthermore, we saw that lamin B was cleaved into 25 and 45 kDa fragments, corresponding to caspase-3 activation during apoptosis (Fig 2G). These experiments further confirmed that destructive proteolytic cleavage is not responsible for lamin B disintegration during nuclear envelope rupture in neutrophils with NET formation.

Nuclear translocation and phosphorylation of PKCα during NET formation

To address how nuclear lamin B was disassembled during nuclear envelope rupture, we found that cytosolic PKCα was translocated to the nuclear membrane where it may mediate lamin B phosphorylation and nuclear envelope disintegration, similar to the role of PKCα during mitosis (Mall *et al*, 2012), and viral infection (Park & Baines, 2006). The immunofluorescent image analysis (Fig 3A) demonstrated that total PKCα was gradually translocated from the cytosol into the nucleus over the time during the early period of PMA stimulation from 5 to 30 min (analysis started after 5 min PMA stimulation to allow the neutrophils to adherer for microscopic analysis). PKCα accumulated in the nucleus and resulted in nuclear envelope discontinuity/rupture at 60-min time point (Fig 3A and B), followed by the consequent extrusion of decondensed chromatin from the ruptured/collapsed nuclear envelope at 180 min (Fig 3A), and the subsequent NET formation. Correspondingly, PKCα phosphorylation was gradually increased over the 3-h stimulation period in human primary pPMNs (Fig 3C and D) and dPMNs (Fig EV1F and G) treated with PMA or PAF.

Accumulation of phosphorylated PKCα in the nucleus results in lamin B phosphorylation, disassembly, and nuclear envelope rupture during NET formation

To explore the potential role of phosphorylated PKCα (p-PKCα) in nuclear envelope rupture, we first isolated the nucleus of neutrophils that were stimulated by PMA at 0 and 2 h (Fig 4A). We found

Figure 2. Nuclear lamin B disassembly, but not proteolytic cleavage, is responsible for nuclear envelope rupture in neutrophils with NET formation.

A, B Representative and summary of immunoblots of full-length lanes of lamin B in human dPMNs that were treated with PMA for 0, 0.5, 1, 2, 3 h during NET formation, or apoptotic dPMNs that were induced by PMA for longer term (12 h) treatment (A).

C, D Representative and summary immunoblots of lamin B in human dPMNs that were treated with PAF for 0, 0.5, 1, 2, 3 h during NET formation.

E Representative confocal microscopy image of a group of pPMNs with NET formation (enclosed by a light blue trapezoid) and their extracellular NETs (indicated by a purple rectangle square) released by these cells, as well as the immunoblot analysis of uncleaved lamin B and cleaved histone H3 with the whole-cell lysates, as well as immunoblot analysis of uncleaved lamin B with lysate of the NETs isolated from conditioned medium of pPMNs with NET formation that were induced by 3 h PMA treatment.

F Representative immunoblots with full-length lanes for lamin B analysis, and pro-caspase-3 and its activated form caspase-3 in human dPMNs with NET formation that were treated with PMA for 0, 0.5, 1, 2, 3 h.

G Representative immunoblots display full-length lamin B (69 kDa) and their cleaved fragments (45 and 25 kDa), and pro-caspase-3 and its activated form caspase-3 in the apoptotic human dPMNs that were treated with PMA for 12, 24 h.

Data information: The anti-human lamin B was used in all immunoblots (A–G) and the confocal image (E), and the latter was further detected by FITC-labeled 2nd Ab, scale bar, 20 μm. Anti-human caspase-3 was used (F, G), and β-actin served as loading control (A–D, F, G). Data represent mean ± SD (n = 3 biological replicates) for (B, D). Comparisons among three or more groups were performed using ANOVA, followed by Student–Newman–Keuls test.
Source data are available online for this figure.

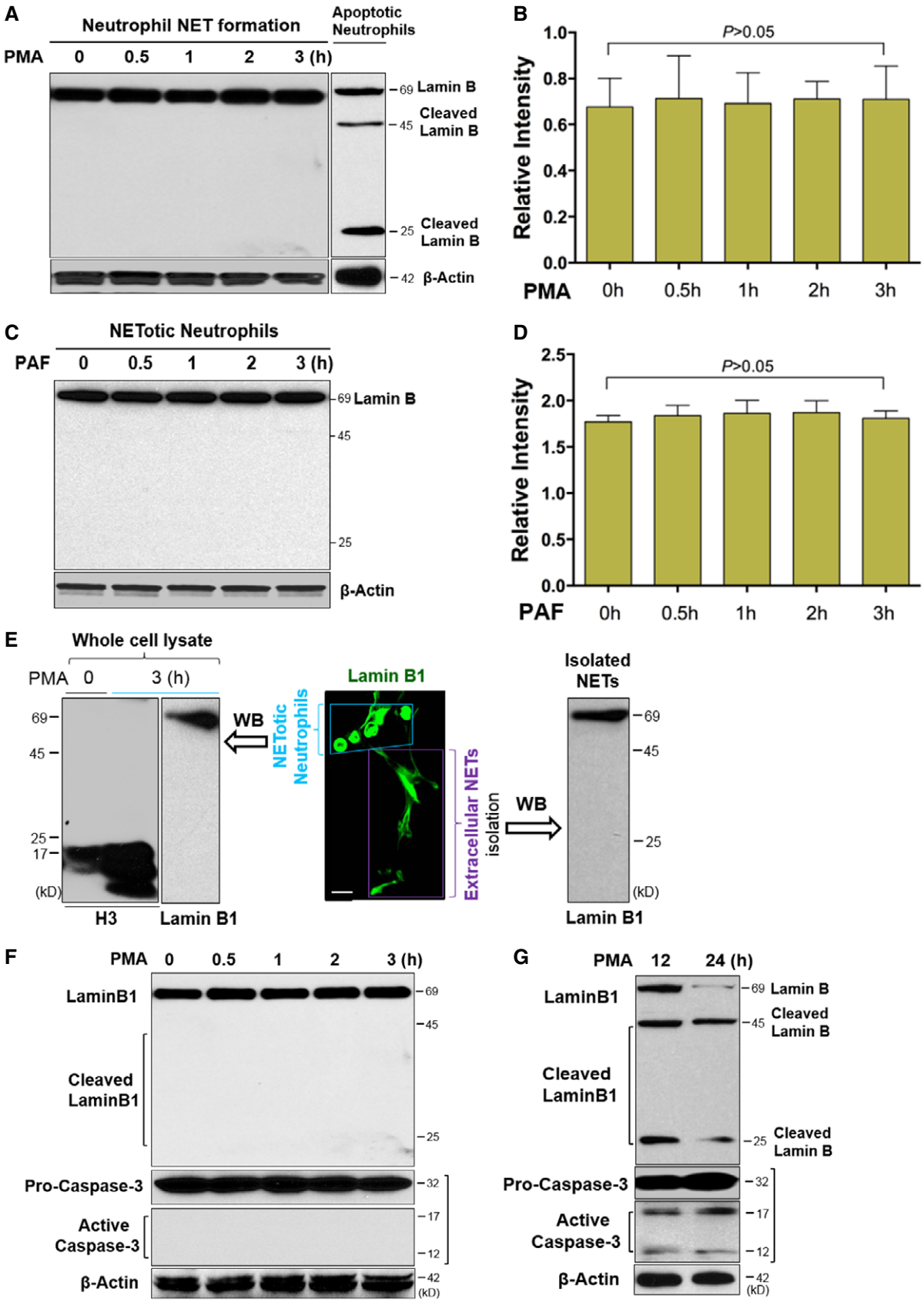
A
Neutrophil NET formation
Apoptotic Neutrophils
PMA 0 0.5 1 2 3 (h)
69 Lamin B
45 Cleaved Lamin B
25 Cleaved Lamin B
42 β-Actin
B
P>0.05
Relative Intensity
PMA 0h 0.5h 1h 2h 3h
C
NETotic Neutrophils
PAF 0 0.5 1 2 3 (h)
69 Lamin B
45
25
β-Actin
D
P>0.05
Relative Intensity
PAF 0h 0.5h 1h 2h 3h
E
Whole cell lysate
PMA 0 3 (h)
69
45
25
17
(kD)
H3
Lamin B1
WB
NETotic Neutrophils
Lamin B1
Extracellular NETs
isolation
WB
Isolated NETs
69
45
25
(kD)
Lamin B1
F
PMA 0 0.5 1 2 3 (h)
LaminB1
Cleaved LaminB1
69
45
25
Pro-Caspase-3
32
Active Caspase-3
17
12
β-Actin
42
(kD)
G
PMA 12 24 (h)
LaminB1
Cleaved LaminB1
69 Lamin B
45 Cleaved Lamin B
25 Cleaved Lamin B
Pro-Caspase-3
32
Active Caspase-3
17
12
β-Actin
42
(kD)

Figure 2.

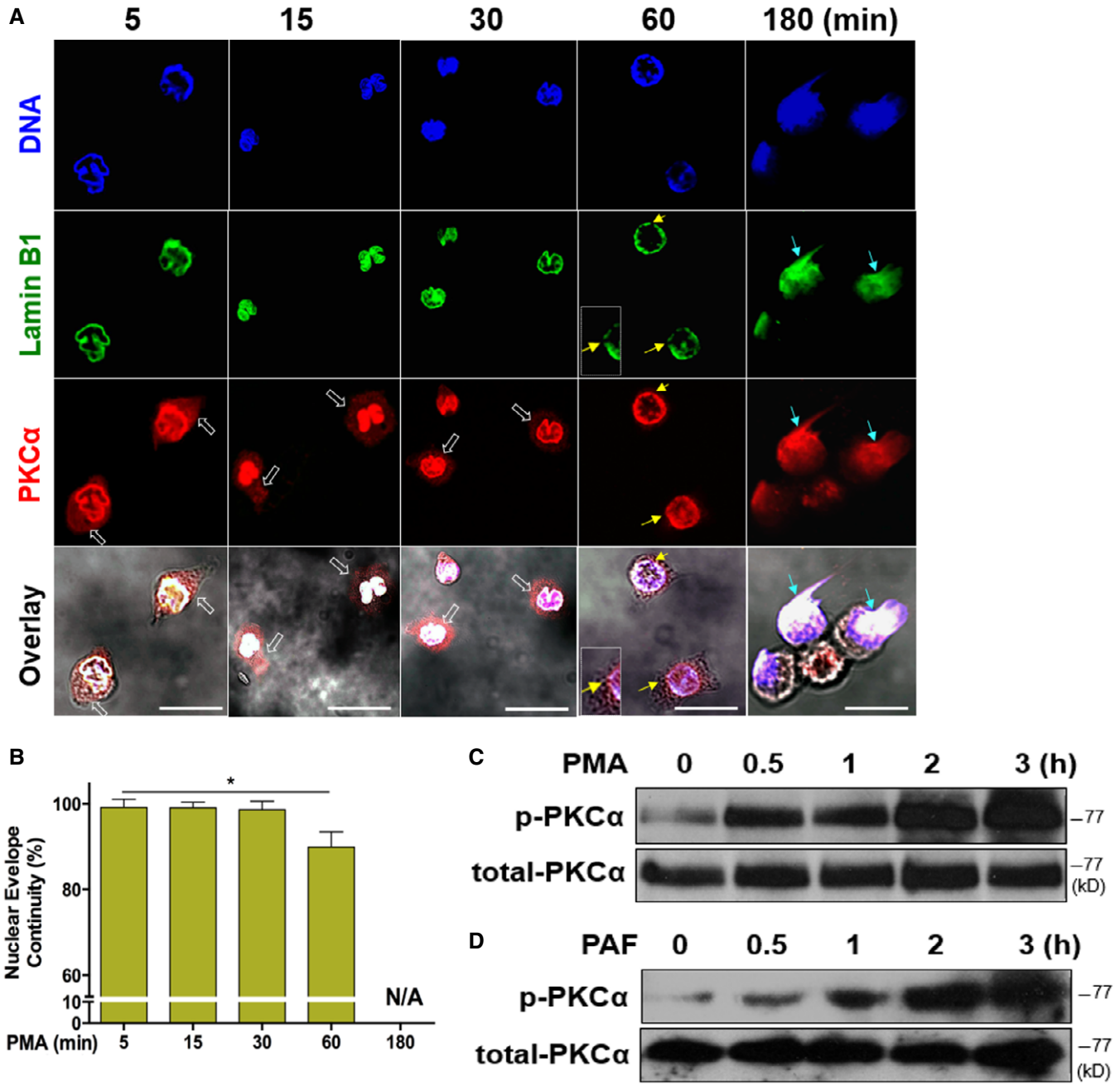

Figure 3. Nuclear translocation and phosphorylation of PKCα is accompanied by nuclear envelope rupture during NET formation.

A Representative images for the time course of PKCα nuclear translocation, subsequent nuclear envelope rupture, and DNA release in human dPMNs exposed to 50 nM PMA for 5, 15, 30, 60, and 180 min and then stained concomitantly for DNA (DAPI), nuclear lamin B (primary anti-lamin B, and FITC-labeled secondary antibody), and PKCα (primary anti-human PKCα, and PE-labeled secondary antibody), followed by confocal fluorescent microscopy analysis. White empty arrows indicate cytoplasmic distribution of PKCα at 5, 15, and 30 min, yellow arrows indicate site of discontinuity/rupture of nuclear envelope at 60 min, light blue arrows display the sites of nuclear envelope rupture and chromatin release at 180 min (A). Scale bars, 20 μm. The time course started 5 min after PMA stimulation in order to allow the adherence of neutrophils on the bottom of dish for immunocytostaining.

B Summary analysis of the nuclear envelope continuity was analyzed based on staining of the nuclear envelope with primary anti-lamin B, and FITC-labeled secondary antibody.

C, D Representative immunoblots of total PKCα and p-PKCα in primary human pPMNs that were treated by PMA (C) or PAF (D) for 0, 0.5, 1, 2, 3 h.

Data information: The summary analyses of panel (B) were calculated based on the circumferences/perimeters of the cell nuclei of 7–10 cells from different time points from 3 to 6 independent experiments. Data in (B) represent mean ± SD (n = 3–6 biological replicates). *P < 0.05 between groups as indicated. Comparisons among three or more groups were performed using ANOVA, followed by Student–Newman–Keuls test.
Source data are available online for this figure.

accumulation of p-PKCα and full-length lamin B in the nuclear fraction of neutrophils with 2-h PMA stimulation (Fig 4A), while there was no detectable total PKCα in the nuclear fraction of neutrophils at time 0 (Fig 4A) in immunoblot analysis. These data are in line with the results obtained by fluorescent microscopy (Fig 3A). Confocal microscopy analysis of a neutrophil in the early stage of NET formation further confirmed the accumulation of p-PKCα in the nucleus, particularly at the rupture site of the nuclear envelope, which had decondensed/swollen chromatin but not yet released to form extracellular traps (b1 cell, Fig 4B). In contrast, another neutrophil in the same image showed a ruptured nuclear envelope with release of decondensed chromatin as the backbone of NETs that contained the mixture of p-PKCα and disassembled nuclear lamin B (b2 cell, Fig 4B). Furthermore, p-PKCα and full-length lamin B were also detected in the immunoblot of the extracellular NETs isolated from cultured human primary pPMNs (Fig 4C). The results of concomitant detection of these two molecules both by immunofluorescent microscopy (Fig 4B) and immunoblots (Fig 4C) indicate a potential active interaction between p-PKCα and lamin B during nuclear envelope rupture.

In several other contexts of nuclear envelope rupture (Shimizu *et al*, 1998; Machowska *et al*, 2015), nuclear lamin B is disassembled through lamin B phosphorylation. There is no relevant anti-phosphorylated lamin B (phospho-lamin B) antibody available for the direct detection of phospho-lamin B. Here, we purified lamin B through immunoprecipitation and analyzed the protein phosphorylation status with anti-p-Ser/Thr/Tyr antibody. Interestingly, increased phospho-lamin B was detected among total lamin B, purified through immunoprecipitation with anti-lamin B antibody, from neutrophils with NET formation stimulated by PMA (Fig 4D and E) or PAF (Fig EV2A and B), as compared to those from control neutrophils.

Taken together these results indicate that nuclear accumulation of p-PKCα (Fig 4A and B) may be responsible for nuclear lamin B phosphorylation (Figs 4D and E, and EV2A and B), phosphorylation-dependent lamin B disassembly, and nuclear envelop rupture that allows the release of full-length lamin B with decondensed nuclear chromatin during NET formation (Fig 4B).

Decreasing lamin B phosphorylation by PKCα inhibition, or mutation of the phosphorylation sites in lamin B, attenuates NET release

To explore the causal role of lamin B phosphorylation, we found that pretreatment of human neutrophils with Go6976, a selective inhibitor of conventional PKC, attenuated PKCα phosphorylation in human neutrophils that were stimulated by PMA (Fig 5A) or PAF (Fig EV2C). Importantly, inhibition of PKCα by Go6976 also decreased lamin B phosphorylation in neutrophils that were treated with PMA (Fig 5B) or PAF (Fig EV2D), as compared to controls. Furthermore, confocal microscopy analysis showed that pretreatment of neutrophils with Go6976 decreased the nuclear accumulation of p-PKCα and prevented the nuclear envelope disintegration in PMA-stimulated neutrophils (Fig 5C). Consequently, inhibition of PKCα significantly attenuated NET formation of primary human pPMNs that were treated by PMA or PAF (Fig EV2E–H). In addition, pretreatment of RAW264.7 macrophages with the PKCα inhibitor Go6976 attenuated PAF-induced extracellular trap formation (Fig EV2I).

To further define the causal role of PKCα-mediated lamin B phosphorylation in NET formation, we introduced mutations at PKCα-consensus serine phosphorylation sites (S395, S405, S408) of lamin B (Hocevar *et al*, 1993; Mall *et al*, 2012; Machowska *et al*, 2015) by replacement of serine (S) with alanine (A) to prevent PKCα-mediated serine phosphorylation. Mutants were made either with single mutations, or with different combinations of mutations (Fig 5D). We found that PAF-induced NET formation was significantly impaired in dPMNs which were transfected with plasmids containing mutations at all three (S395A/S405A/S408A) or two (S395A/S405A), but not other (S395A, S405A, S408A, S395A/S408A, S405A/S408A), PKCα-consensus serine phosphorylation sites of lamin B, as compared to those transfected with WT lamin B (Fig 5E). In addition, PAF-induced extracellular trap formation was also attenuated in RAW264.7 macrophages that were transfected with plasmids containing mutations at all three (S395A/S405A/S408A), but not fewer (S395A, S395A/S405A), as compared to those transfected with WT lamin B controls (Fig EV3A).

Ultraviolet light exposure is related to various human diseases, including lupus and skin cancer (Damiani & Ullrich, 2016). Recent studies have reported that UV radiation may induce NET formation *in vitro* (Azzouz *et al*, 2018; Zawrotniak *et al*, 2019). To explore if UVB-induced NET formation contributes to UVB-induced skin inflammation *in vivo* in the current study, we set out to study it *in vitro*. We found that exposure of dPMNs to UVB at the dose of 150, but not 30 mJ/cm^2 significantly induced NET formation *in vitro* (Fig EV3B and C). Very interestingly, UVB-induced NET formation was also attenuated in dPMNs that were transfected with plasmids containing mutations at all three (S395A/S405A/S408A), but not two (S395A/S405A), PKCα-consensus serine phosphorylation as compared to WT lamin B controls (Fig EV3D).

All of the above experiments highlight a causal link between PKCα and lamin B phosphorylation, suggesting that PKCα may serve as a lamin kinase to mediate lamin B phosphorylation. This consequently results in lamin B disassembly and nuclear envelope rupture, followed by release of extracellular traps in neutrophils or macrophages upon stimulation.

Genetic deficiency of PKCα decreases lamin B phosphorylation and NET formation in primary mouse neutrophils

Next, we sought to further explore the causal effect of PKCα in lamin B phosphorylation and NET formation by using primary mouse neutrophils from both heterozygous and homozygous PKCα deficient mice (Fig 6A). Firstly, the repeated experiments have shown decreased lamin B phosphorylation of immunopurified lamin B by precipitation from the $PKC\alpha^{-/-}$ bone marrow mPMNs as compared to the WT mPMNs (Fig 6B) without or with PAF treatment. These results further defined that PKCα may serve as a lamin kinase to phosphorylate lamin B during NET formation. Most importantly, we found that both peritoneal (Fig 6C–F) and bone marrow (Fig EV3E) mPMNs from either heterozygous (Fig 6C) or homozygous (Fig 6C–F) PKCα-deficient mice had significantly impaired NET formation detected by fluorometric NET quantification (Fig 6C), endpoint analysis of NET-DNA release index (Fig 6D), and fluorescent imaging analysis (Fig 6E and F). In addition, the protective effects of PKCα deficiency were dose-dependent as less NET formation was seen in neutrophils from homozygous PKCα KO mice as compared to those from heterozygous

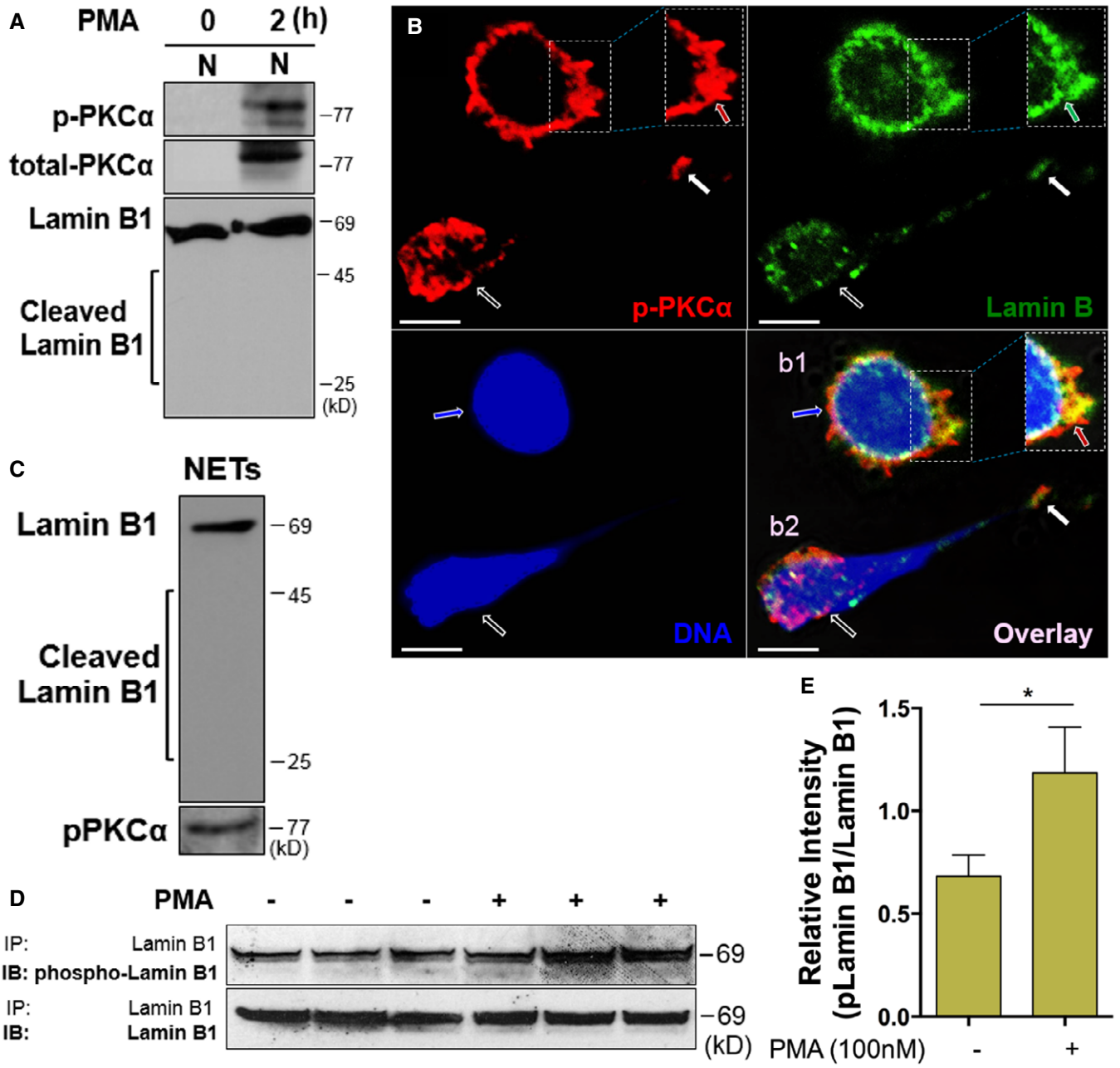

Figure 4. Accumulation of phosphorylated PKCα in nucleus results in nuclear lamin B phosphorylation, disassembly, and the consequent nuclear envelope rupture during NET formation.

A Representative immunoblots of p-PKCα and total PKCα of isolated nuclei and the corresponding status of lamin B in human dPMNs that were treated with PMA for 0 or 2 h.

B Representative sectional images of nuclei of two neutrophils treated by PMA, stained for lamin B (primary anti-lamin B, and FITC-labeled secondary antibody), p-PKCα (primary anti-human p-PKCα^{S657}, and PE-labeled secondary antibody), and nuclear DNA (DAPI). The accumulation of p-PKCα (red arrow pointed) at the site of ruptured/interrupted (green arrow) nuclear lamin B, and swollen/decondensed DNA (blue arrow) were indicated (b1). A neutrophil (white empty arrow) with NET formation that contained the mixture of DNA with p-PKCα and lamin B (white arrow) was also demonstrated (b2). Scale bars, 10 μm.

C Immunoblot images of lamin B, then stripped and probed for p-PKCα, of the homogenates of NETs isolated from conditioned medium of primary human pPMNs with NET formation that were induced by PMA.

D, E Representative and summary immunoblot (IB) detection of phospho-lamin B and total lamin B with the lamin B protein purified by immunoprecipitation (IP) with anti-lamin B from human dPMNs that were treated either by PMA (D, E) for 0 or 3 h. Data represent mean ± SD (n = 3–5 biological replicates) for (E). *P < 0.05 between groups as indicated. Comparison between two groups was analyzed by the Student t test.

Source data are available online for this figure.

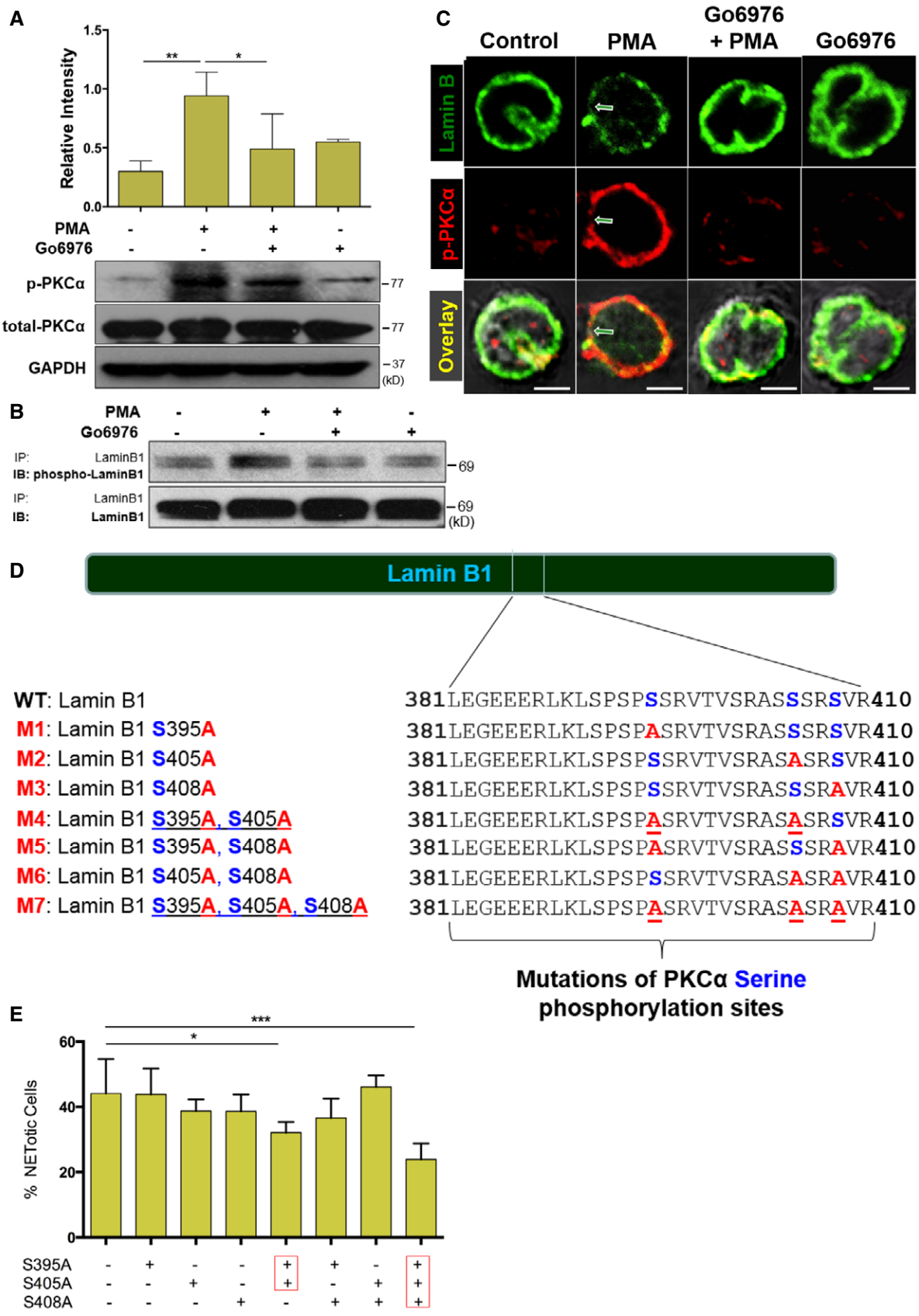
A
Relative Intensity
1.5
1.0
0.5
0.0
**
*
PMA - + + -
Go6976 - - + +
p-PKCα
total-PKCα
GAPDH
77
77
37
(kD)
B
PMA - + + -
Go6976 - - + +
IP: LaminB1
IB: phospho-LaminB1
IP: LaminB1
IB: LaminB1
69
69
(kD)
C
Control
PMA
Go6976 + PMA
Go6976
Lamin B
p-PKCα
Overlay
D
Lamin B1
WT: Lamin B1 381LEGEEERLKLSPSPSSRVTVSRASSSRSVR410
M1: Lamin B1 S395A 381LEGEEERLKLSPSPASRVTVSRASSSRSVR410
M2: Lamin B1 S405A 381LEGEEERLKLSPSPSSRVTVSRASASRSVR410
M3: Lamin B1 S408A 381LEGEEERLKLSPSPSSRVTVSRASSSRAVR410
M4: Lamin B1 S395A, S405A 381LEGEEERLKLSPSPASRVTVSRASASRSVR410
M5: Lamin B1 S395A, S408A 381LEGEEERLKLSPSPASRVTVSRASSSRAVR410
M6: Lamin B1 S405A, S408A 381LEGEEERLKLSPSPSSRVTVSRASASRAVR410
M7: Lamin B1 S395A, S405A, S408A 381LEGEEERLKLSPSPASRVTVSRASASRAVR410
Mutations of PKCα Serine phosphorylation sites
E
***
*
% NETotic Cells
60
40
20
0
S395A - + - - + + - +
S405A - - + - + - + +
S408A - - - + - + + +

Figure 5.

Figure 5. Inhibition of lamin B phosphorylation, or mutation of phosphorylation sites in lamin B, attenuates nuclear envelope rupture and NET release.

A Summary and representative immunoblots of total PKCα and p-PKCα in dPMNs that were pretreated without or with PKC inhibitor Go6976 for 1 h and then treated without or with PMA (A) for 3 h.

B Immunoblot (IB) detection of the phospho-lamin B and total lamin B with lamin B protein purified by immunoprecipitation (IP) with anti-lamin B from human dPMNs that were pretreated without or with PKC inhibitor Go6976 for 1 h and then treated by PMA (B) for 3 h.

C Confocal microscopy images of human dPMNs that were pretreated without or with PKCα Go6976 for 1 h and then treated without or with PMA for 3 h, followed by staining of lamin B (primary anti-lamin B, and FITC-labeled secondary antibody), and phosphorylated PKCα (primary anti-human p-PKCα^{S657}, and PE-labeled secondary antibody). The green/white arrows indicate the site of nuclear envelope rupture. Scale bars, 10 μm.

D Schematic representation of lamin B domain structure and several mitotic serine phosphorylation sites (indicated by blue font) that exhibit PKC consensus motifs (Mall *et al*, 2012) and overview of lamin B reporters containing serine (S) to alanine (A) mutations at PKC consensus phosphorylation sites.

E The endpoint analysis of % cells with NET formation was detected with dPMNs that were transfected with plasmids of either wild-type lamin B (WT control) or mutants with single or multiple defined point mutations at PKCα-consensus phosphorylation sites (S395A, S405A, S408A) of lamin B, and treated for 3 h by 10 μM PAF in medium containing cell-permeable dye SYTO Red (500 nM) for the total cell count, while the cells with NET formation were stained by cell-impermeable dye SYTOX Blue (5 μM). Then, the images were taken with Olympus confocal microscopy, followed by automated quantification of NETs using ImageJ for quantification of % cells with NET formation.

Data information: Panels (A) is summary analyses of immunoblots that were calculated based on the arbitrary unit (A), or percentage of cells with NET formation by immunofluorescent imaging quantification using ImageJ (E), from 3 to 5 independent experiments. Data represent mean ± SD (n = 3–5 biological replicates). *P < 0.05, **P < 0.01, ***P < 0.001, between groups as indicated. Comparisons among three or more groups were performed using ANOVA, followed by Student–Newman–Keuls test.
Source data are available online for this figure.

PKCα-deficient mice (Figs 6C and EV3E). Our results from the genetic PKCα deficient mice provide important evidence that PKCα is crucial to NET formation, at least in part, by serving as a lamin kinase to regulate phosphorylation and disassembly of lamin B during nuclear envelope rupture and NET formation in neutrophils.

Strengthening nuclear envelope integrity by lamin B overexpression attenuates NET release *in vivo* and reduces NET-associated proinflammatory cytokines in UVB-irradiated skin of lamin B transgenic mice

After identifying a crucial role of lamin B integrity in NET formation *in vitro* (Fig 1E–H), we next sought to examine if the same mechanism is also acting *in vivo*. IHC staining demonstrated extensive extrusion of decondensed chromatin in neutrophils in skin tissues of UVB-irradiated WT mice (Fig 7A). In contrast, we observed fewer neutrophils, particularly neutrophils without externalization of citrullinated chromatin (anti-Cit-H3 staining), in UVB-irradiated skin of Lmnb1^{TG} mice (Fig 7B). Therefore, these *in vivo* results confirm the findings from the *in vitro* experiments (Fig 1E–H), in which strengthening nuclear envelope integrity by lamin B overexpression attenuated NET formation. The summary analysis demonstrates that NET formation and neutrophil infiltration was attenuated in UVB-irradiated skin of Lmnb1^{TG} mice as compared to those of WT littermates (Figs 7C and EV4A). Furthermore, neutrophils with NET formation exhibited proinflammatory cytokines, IL-17A and TNFα, in UVB-irradiated skin of WT littermates (Figs 7D and E, and EV4B–E). Very interestingly, we found attenuated NET release with decreased levels of NET-associated cytokines in UVB-irradiated skin of Lmnb1^{TG} mice (Figs 7C–E and EV4A–E) compared to WT littermates. In the current study, we used both anti-Ly6B (Nakazawa *et al*, 2017; Fig 7A–E) and anti-Ly6G (Amulic *et al*, 2017; Fig EV4A–E) to detect neutrophils as reported by other publications (Amulic *et al*, 2017; Nakazawa *et al*, 2017).

To understand the decreased numbers of neutrophils with NET formation in skin of UVB-irradiated Lmnb1^{TG} mice, we also examined if nuclear lamin B overexpression affects the neutrophil counts in the peripheral blood and the neutrophil transmigration ability,

Figure 6. Genetic deficiency of PKCα attenuates lamin B phosphorylation and NET formation in primary neutrophils from PKCα knockout mice.

A Summary and representative immunoblots of PKCα expressions in mouse bone marrow neutrophils from PKCα$^{-/-}$, PKCα$^{+/-}$, and their littermate WT (PKCα$^{+/+}$) mice. Vinculin served as loading control.

B Representative immunoblot (IB) detection of the phospho-lamin B (Ser) and total lamin B with lamin B protein purified by immunoprecipitation (IP) with anti-lamin B from mouse peritoneal mPMNs from WT vs. PKCα$^{-/-}$ mice, stimulated without or with PAF for 3 h.

C Summary analyses of NET formation in peritoneal mPMNs, from WT, PKCα$^{+/-}$, or PKCα$^{-/-}$ mice, which were treated without or with either 5 μM or 10 μM PAF for 3 h following by 2% PFA fixation and fluorometric microplate analysis.

D The endpoint analysis of NET-DNA release index was detected by coincubation of primary mouse peritoneal mPMNs from WT and PKCα$^{-/-}$ mice without (control) or with 10 μM PAF in medium containing 1 μM SYTOX Green dye with recording by a microplate reader at the end of the 3 h time point. The NET-DNA release index was reported in comparison with an assigned value of 100% for the total DNA released by neutrophils lysed by 0.5% (*v*/*v*) Triton X-100.

E, F (E) Representative and (F) summary analysis of NET formation of mouse peritoneal mPMNs from WT vs. PKCα$^{-/-}$ mice stimulated without or with 10 μM PAF for 3 h and stained with both cell-permeable SYTO Red dye and cell-impermeable SYTOX Green dye, without fixation. Images were taken by Olympus confocal microscopy, followed by automated quantification of NETs on 5–6 non-overlapping area per well using ImageJ for calculation of % cells with NET formation. (E) Scale bars, 50 μm.

Data information: Panels (A, C, D, F) were summary analyses that were calculated based on the arbitrary unit (A) or arbitrary fluorescent readout (C), endpoint analysis of NET-DNA release index (D), or % cells with NET formation by image analysis using ImageJ (F) from 3 to 6 independent experiments as compared to their WT or untreated controls. Data represent mean ± SD (n = 3–6 biological replicates), *P < 0.05, **P < 0.01 between groups as indicated. Comparisons among three or more groups were performed using ANOVA, followed by Student–Newman–Keuls test.
Source data are available online for this figure.

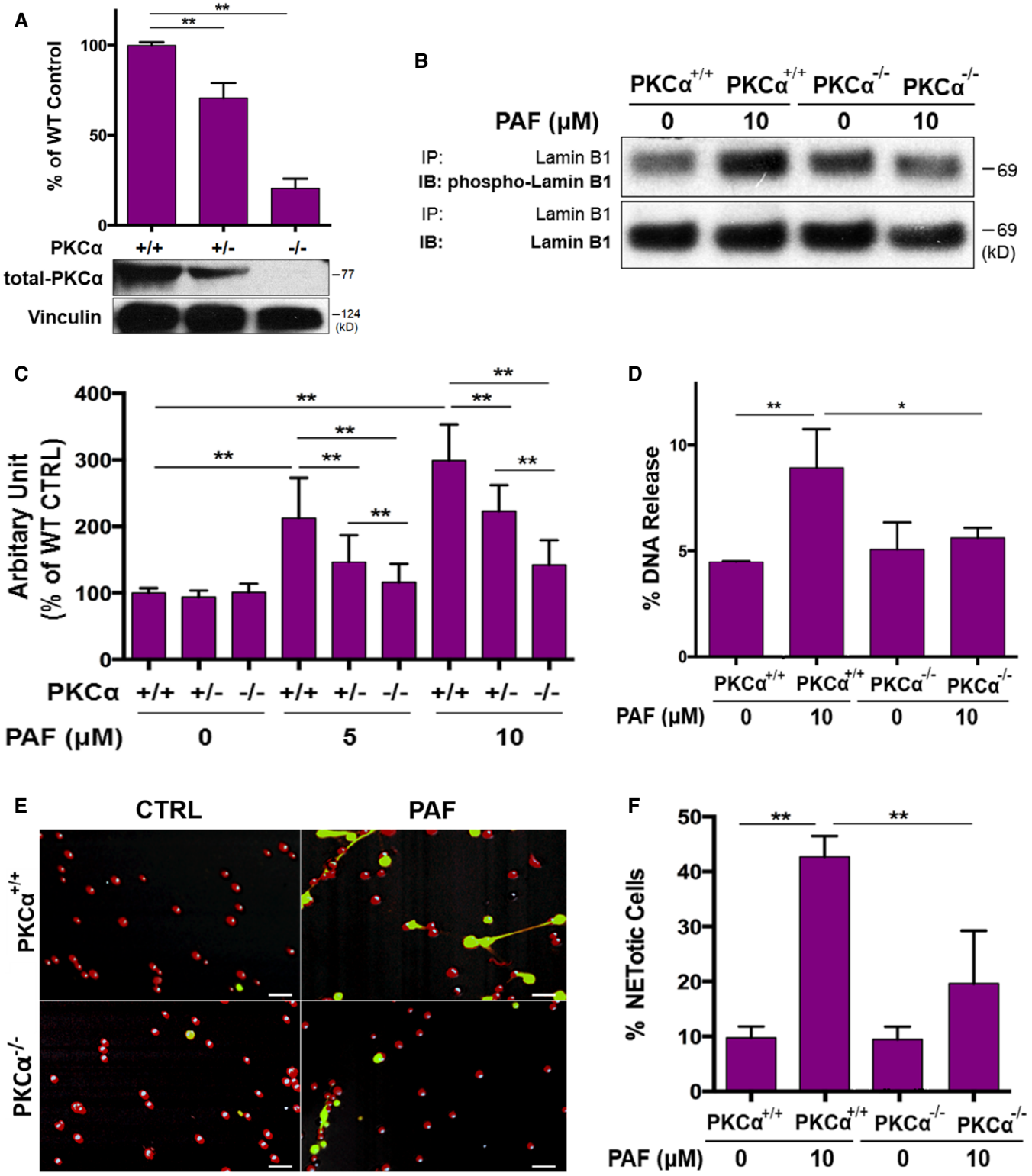

Figure 6.

which may influence the amount of neutrophil recruitment to inflamed skin. No significant differences were detected for either neutrophil counts in peripheral blood (Fig EV5A), or pore transmigration ability of neutrophils (Fig EV5B), from the Lmnb1^{TG} vs. WT mice. Therefore, neither the normal neutrophil counts, nor the unaffected transmigration ability, may contribute to the decreased neutrophil accumulation in the skin tissues of UVB-irradiated Lmnb1^{TG} mice as compared to those of WT control mice (Fig 7C).

It has been known that IL-17A and TNFα can synergistically work to sustain neutrophil recruitment during inflammatory responses (Liu *et al*, 2011; Griffin *et al*, 2012). Thus, one may propose that the exhibition of IL-17A and TNFα by NETs may propagate neutrophil recruitment to inflamed skin of UVB-irradiated mice. To address this point, we found reduced exhibition of NET-associated IL-17A and

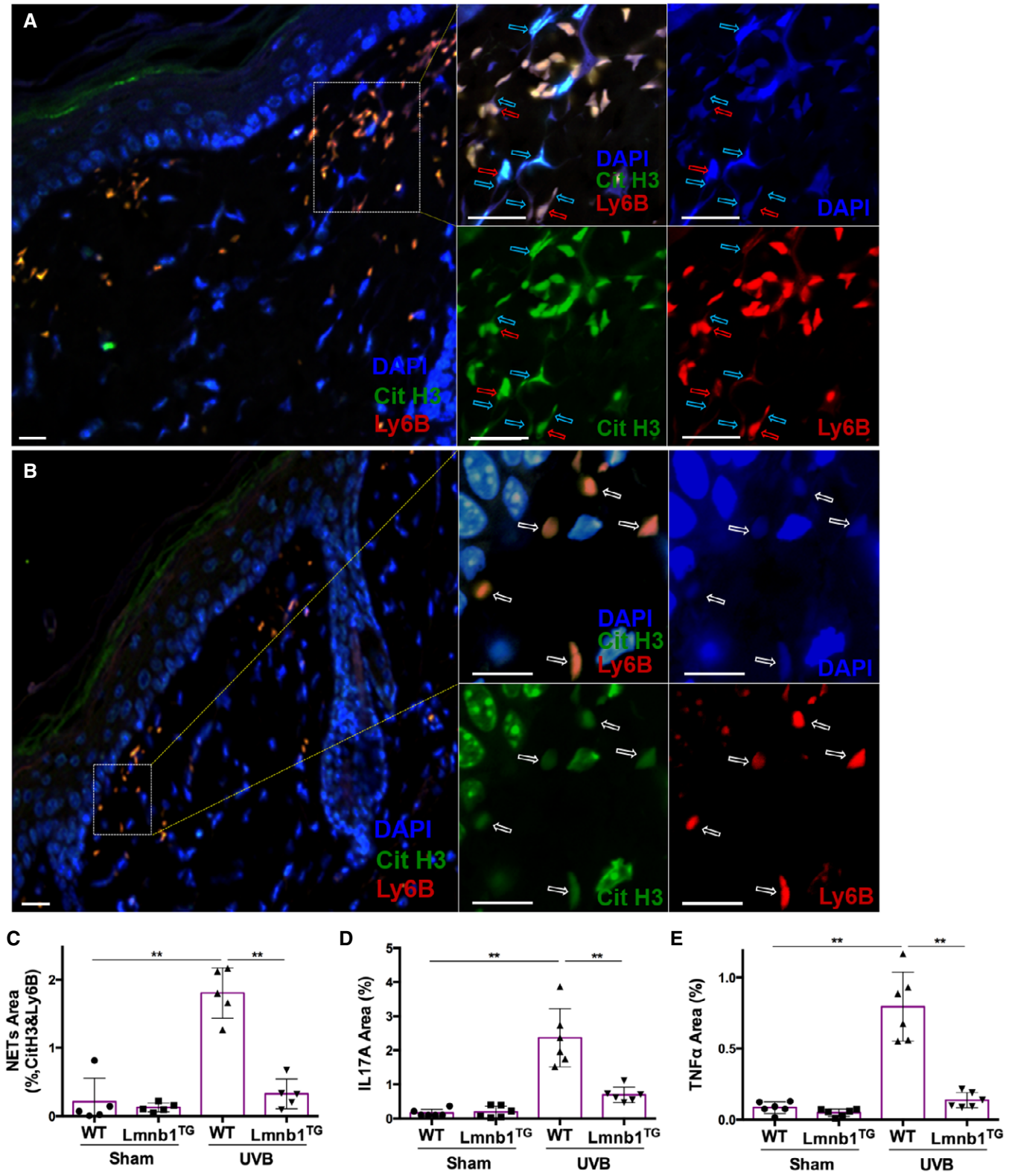

Figure 7.

Figure 7. Strengthening nuclear envelope integrity by lamin B overexpression decreases NET release *in vivo* and alleviates NET-associated proinflammatory cytokine accumulation in UVB-irradiated skin of the lamin B transgenic mice.

A–C (A, B) representative (C) summary analysis of confocal fluorescent microscopy images of neutrophils with NET formation in the skin tissue of WT (A) vs. Lmnb1^{TG} (B) mice with UVB exposure, in which DNA was stained by DAPI, citrullinated histone H3 was probed by rabbit anti-mouse citrullinated histone H3, following stained by Alexa Fluor-488-labeled donkey anti-rabbit secondary antibody, while neutrophil surface marker Ly6B was probed by rat anti-mouse Ly6B Ab following stained by Alexa Fluor-647-conjugated goat anti-rat secondary antibody. The images of different staining and their overlays are shown (A, B). The parental neutrophils (stained by neutrophil membrane surface marker Ly6B) and their released extracellular NET structures (co-stained by anti-cit H3 and DAPI) are indicated by red arrows and light blue arrows, respectively. The white arrows indicated neutrophils without NET release. Scale bar, 50 μm.

D, E Summary analysis for staining area of neutrophils with NET formation and their exhibition of IL-17A (D) or TNFα (E), in the skin tissue of WT vs. Lmnb1^{TG} mice without (sham) or with UVB exposure, by co-staining of Ly6B (stained as described in panels A–C) with IL-17A (D) or TNFα (E) using FITC-conjugated rat anti-mouse IL-17A, or FITC-conjugated rat anti-mouse TNFα Abs.

Data information: DNA was stained by DAPI. Panels (C–E) are summary analyses that were calculated based on the arbitrary fluorescent unit (C–E) from 5 to 6 independent experiments of different groups as indicated. Data represent mean ± SD (n = 5–6 biological replicates). $^{**}P < 0.01$ between groups are indicated. Comparisons among three or more groups were performed using ANOVA, followed by Student–Newman–Keuls test.

TNFα in skin tissue of UVB-irradiated Lmnb1^{TG} mice as compared to those of WT mice (Figs 7D and E, and EV4B–E). In the *in vitro* study, we found the expression of IL-17A and TNFα in PAF-stimulated neutrophils from both Lmnb1^{TG} vs. WT mice, and the exhibition of these cytokines by NETs of neutrophils from WT mice (Fig EV5C and D). These *in vitro* experimental results indicate that neutrophils from both Lmnb1^{TG} vs. WT mice can express IL-17A and TNFα that are known to diffuse freely from local tissue to the circulation and then diluted. In contrast, NET-associated cytokines can be retained in local microenvironment with a relatively high concentration, thus synergistically contributing to the sustained neutrophil recruitment to inflamed skin. Thus, reduced NET formation with decreased extracellular display of IL-17A and TNFα may, at least in part, explain the attenuated neutrophil recruitment to UVB-irradiated skin in Lmnb1^{TG} mice as compared to that in WT littermates.

The results from *in vitro* and *in vivo* studies have verified our hypothesis that lamin B is crucial to nuclear envelope integrity, and strengthening nuclear envelope integrity by lamin B overexpression attenuated NET release in lamin B transgenic mice.

Discussion

Externalization of decondensed chromatin from the ruptured nuclear envelope forms the backbone of NETs. Lamin B filamentous meshwork is a substantial structural component of the nuclear envelope. Given the nature of their structural arrangement, lamin B filaments are assembled laterally to form a highly organized meshwork underneath the inner nuclear membrane. The two are vertically associated by the integral membrane protein LBR (Fig 1C; Vergnes *et al*, 2004; Goldberg *et al*, 2008). The role of nuclear lamin B in neutrophil biology and its involvement in nuclear envelope rupture and NET formation has not been investigated, although LBR has been used as a marker of the nuclear envelope in neutrophil biology studies (Fuchs *et al*, 2007; Singh *et al*, 2016). Here, we verified that nuclear lamin B is involved, and the disassembled lamin B is also released and decorated on the surface of externalized NET structures. To test the effects of nuclear lamin B, we found that overexpression of lamin B strengthened the nuclear envelope integrity and blunts NET release *in vitro*. In contrast, the reduced amount of mature lamin B both in neutrophils and macrophages, by inhibition of protein farnesylation with farnesyltransferase inhibitor (FTI) (Adam *et al*, 2013), can enhance NET release in these cells. Taken together, the levels of nuclear lamin B expression affect nuclear envelope integrity and NET formation in a negative dose-dependent manner. Therefore, our findings provide compelling evidence for the importance of lamin B in the nuclear envelope integrity and NET formation. In line with our findings, a recent study reported that nuclear lamin A/C is also involved in NET formation (Amulic *et al*, 2017).

During nuclear envelope rupture, nuclear lamin B is either cleaved or disassembled (Hocevar *et al*, 1993; Collas *et al*, 1997; Slee *et al*, 2001) in different cellular events. According to the lytic cell death mechanism of NET formation described before (Fuchs *et al*, 2007; Papayannopoulos *et al*, 2010; Yipp & Kubes, 2013), we expected to see the destructive proteolytic cleavage of lamin B during NET formation. However, we only found the intact full-length lamin B both in whole-cell lysates and the isolated NETs. These unexpected results indicated that this nuclear structural protein was not destructively cleaved during NET formation. In contrast, lamin B in apoptotic neutrophils was indeed fragmented, through proteolytic cleavage by the activated caspase-3 (Slee *et al*, 2001). In our study, the pro-caspase-3 remained as an inactive molecule throughout the period of NET formation. Our results are in line with a previous report in which NET formation is a caspase-independent process (Remijsen *et al*, 2011). All of the above results support the proteolytic-independent mechanism of lamin B disassembly during NET formation. Cyclin-dependent kinases (CDK) 4/6 have been reported to be involved in NET formation through lamin A/C phosphorylation (Amulic *et al*, 2017). In addition, nuclear swelling and chromatin decondensation via histone citrullination (Wang *et al*, 2009) or acetylation (Hamam *et al*, 2019) provides physical force to drive nuclear envelope rupture and chromatin release (Neubert *et al*, 2018). Furthermore, a few recent studies reported that Gasdermin D may also contribute to nuclear expansion, nuclear envelope rupture, and NET release (Chen *et al*, 2018; Sollberger *et al*, 2018). Taken together, these latest novel findings from our and other groups (Amulic *et al*, 2017; Chen *et al*, 2018; Neubert *et al*, 2018; Sollberger *et al*, 2018; Hamam *et al*, 2019) suggest that nuclear envelope rupture appears to be a distinct process from previously described (Fuchs *et al*, 2007; Papayannopoulos *et al*, 2010; Yipp & Kubes, 2013).

Assembly of the monomeric lamin proteins (lamin A/C, B) is required for the formation of fibrous meshworks and maintenance of the nuclear envelope integrity (Vergnes *et al*, 2004; Goldberg *et al*, 2008). To explore the potential mechanisms of lamin B disassembly, we found that cytosolic PKCα was translocated to nucleus where it became activated and phosphorylated, probably by

diacylglycerol (DAG) derived from the nuclear membrane (Neri *et al*, 1998; Martelli *et al*, 2006). Nuclear DAG may act as a chemoattractant to induce nuclear translocation and activation of PKCα (Neri *et al*, 1998; Martelli *et al*, 2006), while nuclear lamin B serves as a PKCα substrate for its nuclear localization (Neri *et al*, 1998; Martelli *et al*, 2006). Nuclear accumulation of activated PKCα, i.e., p-PKCα^{Ser657} (Bornancin & Parker, 1997), is responsible for lamin B phosphorylation, phosphorylation-dependent disassembly (Hocevar *et al*, 1993), and consequent nuclear envelope rupture. In the current study, co-localization of p-PKCα and lamin B in the nucleus would make it possible for their direct interaction and phosphorylation of lamin B, while phosphorylation results in lamin B disassembly and efficient nuclear envelope breakdown (Collas *et al*, 1997; Mall *et al*, 2012). In addition, the coexistence of p-PKCα and lamin B in the released extracellular NETs further indicate their possible interaction happened in the nucleus.

To determine the causal role of PKCα, we found that either pharmacological inhibition, or genetic deficiency, of PKCα inhibited lamin B phosphorylation, resulting in attenuated nuclear envelope rupture and NET formation. Most importantly, mutation at three PKCα-consensus serine phosphorylation sites of lamin B impaired the release of extracellular traps both in neutrophils and macrophages, indicating a causal role of PKCα-mediated lamin B phosphorylation in lamina disassembly and nuclear envelope rupture during NET formation. The above findings with independent experimental approaches provide strong evidence for the causal role of PKCα-mediated lamin B phosphorylation in NET formation. In addition to PKCα, PKCβII may also be involved in NET formation as Go6976 is known to inhibit both PKCα and PKCβ, and PKCβII is known to phosphorylate lamin B (Martelli *et al*, 2006). In line with us, the PKCβ-specific inhibitor LY333531 is also reported to inhibit NET formation *in vitro* (Chen *et al*, 2018).

PKCs regulate the function of proteins through phosphorylation of hydroxyl groups of serine and threonine amino acid residues on these proteins (Fontayne *et al*, 2001). The current study indicates that PKCα can phosphorylate several serine sites (S395/S405/S408) of lamin B, resulting in lamin B disassembly. Fontayne *et al* (2001) reported that several PKCs (i.e., PKCα) can indirectly induce ROS production through NOX activation by phosphorylation of serine (probably S328) of the NOX p47^{phox} subunit. So, both lamin B and p47^{phox} are substrates for PKC-mediated phosphorylation (Collas *et al*, 1997; Fontayne *et al*, 2001). Lamin B phosphorylation is the direct effect of PKCα in the nucleus, while ROS generation is an indirect effect of PKCα through activation of NOX2 in cell membrane (Fontayne *et al*, 2001); thus, the two distinct cellular events seem to take place in different cellular compartments during the multi-step process of NET formation. Given PKCα-mediated nuclear lamina disassembly may be essential to nuclear chromatin extrusion from the broken nuclear envelope during NET formation, while NOX2-mediated ROS is only involved in some (Fuchs *et al*, 2007; Papayannopoulos *et al*, 2010; Douda *et al*, 2015), but not all (Rochael *et al*, 2015; Pieterse *et al*, 2018; Tatsiy & McDonald, 2018), types of NET formation through different mechanisms (Fuchs *et al*, 2007; Papayannopoulos *et al*, 2010; Douda *et al*, 2015). Thus, one may propose that the direct effects of PKCα on nuclear lamin B phosphorylation is required, but the indirect effects of PKCα through NOX-ROS pathway may not be necessary, to the nuclear envelop rupture during NET formation. Similarly, Zychlinsky's group reported that CDK4/6 can control NET formation through phosphorylation of lamin A/C (Amulic *et al*, 2017), while lamin A/C can still be phosphorylated in NOX2-deficient neutrophils from patients with chronic granulomatous disease (Amulic *et al*, 2017). Thus, they suggest that the cell-cycle signaling CDK4/6 may function in a parallel pathway to ROS generation during NET formation (Amulic *et al*, 2017). Taken together, nuclear lamina phosphorylation (for lamin A/C, and B) by either CDK4/6 or PKCα, and cytosolic ROS generation by NOX2, might be independent cellular events during NET formation (Amulic *et al*, 2017).

In addition to identifying the crucial role of lamin B in NET formation *in vitro*, we also tested it *in vivo* by studying NET formation in skin inflammation induced by UVB exposure, a risk factor for lupus and skin cancer (Damiani & Ullrich, 2016). We confirmed the crucial role of lamin B in nuclear envelope integrity and NET formation *in vivo* as neutrophils in UVB-irradiated skin of Lmnb1^{TG} mice exhibited a lack of NET formation. Regarding the relevant mechanisms, UVB exposure is known to stimulate skin keratinocytes to release PAF (Damiani & Ullrich, 2016), a natural proinflammatory lipid mediator that can induce NET formation (Etulain *et al*, 2015). The current study suggests that PAF might be a potential natural stimulus for NET formation in UVB-irradiated skin. Furthermore, the current study and few recent publications demonstrated that UV could induce NET formation *in vitro* in cultured neutrophils (Azzouz *et al*, 2018; Neubert *et al*, 2019; Zawrotniak *et al*, 2019). Therefore, UVB-induced NET formation *in vivo* may be attributed to the indirect effect of UVB through PAF (Etulain *et al*, 2015; Damiani & Ullrich, 2016) and the direct effects of UVB light on neutrophils that have been recruited to the inflamed skin (Zawrotniak *et al*, 2019).

The externalization of NETs may be important for the propagation of inflammation by induction of proinflammatory cytokines (Lood *et al*, 2016). Studies have shown that UVB irradiation can induce IL-17A (Li *et al*, 2015) and TNFα (Sharma *et al*, 2011), both of which can be expressed by neutrophils (Lin *et al*, 2011; Giambelluca *et al*, 2014). In the current study, we found that NETs exhibited both IL-17A and TNFα in the skin of UVB-irradiated WT mice. Co-presence of IL-17A and TNFα on NETs may synergistically propagate inflammatory responses through different mechanisms (Ruddy *et al*, 2004; Liu *et al*, 2011; Griffin *et al*, 2012). Interestingly, the current study showed that strengthening nuclear envelope integrity attenuated NET formation *in vivo* in Lmnb1^{TG} mice. Those neutrophils enclosed IL-17A and TNFα within the cells, thus decreasing the opportunity for their exhibition by NETs to the extracellular milieu. Therefore, the intracellular retention, but not extensive extracellular display, of cytokines by neutrophils without NET release may prevent further propagation of inflammatory responses in UVB-irradiated Lmnb1^{TG} mice. On the other hand, the neutrophil numbers in blood may not contribute to the decreased leukocyte infiltration in the skin of UVB-irradiated Lmnb1^{TG} mice since lamin B overexpression does not affect neutrophil counts in blood.

It is known that the stiffness of nuclei may affect the transmigration capability of cells (Lammerding *et al*, 2006; Goldberg *et al*, 2008; Rowat *et al*, 2013). Published papers demonstrated that A-type lamins, but not B-type lamins, contribute to the mechanical stiffness of nuclei (Lammerding *et al*, 2006; Goldberg *et al*, 2008; Rowat *et al*, 2013), and the nuclear stiffness increases with the lamin A:B ratio (Shin *et al*, 2013). Increasing the lamin A:B ratio by downregulation of lamin B promotes nuclear stiffness in

hematopoietic cells (Shin *et al*, 2013). Thus, elevated lamin B expression may not increase nuclear stiffness in neutrophils and influence their migration to inflamed skin in Lmnb1^{TG} mice. Therefore, reduced NET release with decreased extracellular cytokine exhibition may explain, at least in part, the attenuated skin inflammation in UVB-irradiated Lmnb1^{TG} mice. Nevertheless, the current study was mainly focused on the novel molecular and cellular mechanism, while the animal study was designed to test the mechanism *in vivo*. To thoroughly understand the role of NET formation in driving skin inflammation in Lmnb1^{TG} mice following UVB irradiation, an additional study may be needed to examine NET-stimulated production of cytokines other than IL-17A and TNFα, and their effects on skin inflammation, as well as the neutrophil-independent changes, i.e., keratinocytes and other inflammatory cells. In addition to UVB-irradiation models, other animal models (Brinkmann *et al*, 2004; Lood *et al*, 2016; Martinod *et al*, 2016) may also be used to test the role of nuclear lamina integration in NET formation *in vivo* in the future.

In conclusion, our novel findings identified that (i) lamin B is crucial to the nuclear envelope integrity in neutrophils, (ii) PKCα serves as lamin kinase that mediates lamin B phosphorylation, resulting in consequent nuclear envelope rupture and NET formation, and (iii) strengthening nuclear envelope integrity by lamin B overexpression attenuates NET formation *in vitro* and *in vivo*, thus alleviating the release of NET-associated cytokines in the skin of UVB-irradiated lamin B transgenic mice. These findings, combined with other recent studies (Amulic *et al*, 2017; Neubert *et al*, 2018), advance our mechanistic understanding of NET formation. The current work highlights a cellular mechanism in nuclear envelope rupture during NET formation, which may provide avenues towards new therapeutic strategies for NET-associated human diseases.

Materials and Methods

Mice

Lamin B1 transgenic C57BL/6J-Tg (Lmnb1^{TG}) 1Yfu/J mice (JAX stock #023083) (Heng *et al*, 2013), PKCα-deficient mice (B6;129-Prkca ^{tm1Jmk}/J mice, JAX stock #009068) (Braz *et al*, 2004), and their corresponding littermate controls were housed in a pathogen-free environment and given food and water *ad libitum*. All the animal experiments were approved by the Animal Care and Use Committee of Philadelphia VA Medical Center.

Cell culture and treatment

Primary human polymorphic nuclear granulocytes (pPMNs) or neutrophils were isolated by *dextran* (250,000) sedimentation of red blood cells (RBC) followed by Ficoll-Paque PLUS H-1077 (GE Healthcare) gradient separation as described before with modification (Denny *et al*, 2010). Primary mouse peritoneal and bone marrow neutrophils (mPMNs) were isolated according to the published protocols (Boxio *et al*, 2004). Mouse peritoneal mPMN isolation was conducted with 3% thioglycollate broth (TGB) medium induction and then isolated with neutrophil isolation kit (Miltenyl) according to manufacturer's instruction. Mouse bone marrow mPMNs were isolated from the *femur* and *tibia* bone marrow with a neutrophil isolation kit (Miltenyl). PKCα-deficient mPMNs were isolated from heterozygous (PKCα$^{+/-}$) or homozygous (PKCα$^{-/-}$) PKCα-deficient mice (B6;129-Prkca ^{tm1Jmk}/J mice, JAX stock #009068) (Boxio *et al*, 2004).

The mPMNs with lamin B overexpression (Lmnb1^{TG}) were isolated from lamin B1 transgenic C57BL/6J-Tg (LMNB1) 1Yfu/J mice (JAX stock #023083) (Heng *et al*, 2013). Neutrophils from their littermate wild-type (WT) control mice for both PKCα deficient and lamin B1 transgenic strains served as controls. Mouse peripheral blood neutrophil counts for Lmnb1^{TG} vs. WT mice were conducted using May–Grunwald–Giemsa staining of the peripheral blood smear slides, and total white blood count was analyzed with methylene blue and acetic acid, with commercial kits according to manufacturers' protocols. The pore transmigration study of the neutrophils from Lmnb1^{TG} vs. WT mice was conducted as described before (Justus *et al*, 2014) by using Boyden chamber, 24-well transwell plates with 3 μm pore inserts, under stimulation of PAF (10 μM). The pore transmigration ability in neutrophils from the Lmnb1^{TG} mice was expressed as relative transmigration compared to that in neutrophils from WT littermates.

Human HL-60 cell line was differentiated into neutrophil-like or polymorphic nuclear granulocytes (dPMNs) in RPMI-1640 with 10% FBS and 1.2% DMSO for 5–6 days as described in our published work (Folkesson *et al*, 2015). RAW264.7 cells (ATCC) were cultured in DMEM medium supplemented with 10% FBS and were also used in certain experiments. All of the above pPMNs, dPMNs, mPMNs, or RAW264.7 were treated with PMA (50 or 100 nM) or PAF (5 or 10 μM) for 0–3 h without or with 1-h pretreatment with an inhibitor of conventional PKC Go6976, followed by detection of NET formation, or lysis for immunoblot analysis. Since lamin B maturation is regulated by farnesylation (Adam *et al*, 2013), the reduced mature lamin B expression in HL-60 dPMNs or RAW264.7 cells was achieved by treatment without (0) or with 2 or 10 μM farnesyltransferase inhibitor (FTI) L-744,832 for 48 h. In addition, we also examined the effects of UVB radiation on NET formation *in vitro* (Azzouz *et al*, 2018; Zawrotniak *et al*, 2019), using our published protocol (Bashir *et al*, 2009) with modifications. In brief, dPMNs were placed into a poly-D-lysine-coated 48-well plate that was irradiated at the top of the plate with a dose of 30 (Bashir *et al*, 2009) or 150 mJ/cm^2 with two FS40T12-UVB bulbs (Bashir *et al*, 2009). Then, NET formation was determined either by kinetic analysis for up to 6 h or by immunofluorescent imaging quantification analysis of the fixed cells 6 h later.

NET formation assessment and quantification

All of the above pPMNs, dPMNs, or mPMNs were treated with either PMA (50 or 100 nM) or PAF (5 or 10 μM), for 0–3 h. Three currently validated methodologies were used for NET formation assessment and quantification in the current study. (i) In the conventional fluorometric NET quantification (Sollberger *et al*, 2016), the above treated or untreated cells were fixed with 2% PFA after the stimulation and stained with 1 μM SYTOX Green, following by fluorescent readout with a microplate reader at 485/518 nm as described before with modification (Sollberger *et al*, 2016). NET formation in each experiment was also confirmed by fluorescent microscopy. (ii) For measuring the NET-DNA release index under different conditions (Douda *et al*, 2015; Khan *et al*, 2018), cells were

grown without (control) or with PMA or PAF treatment for 3 h in medium containing 1 μM SYTOX Green dye in 48-well plates. The experiments were recorded by a microplate reader either at the end of the 3-h treatment for endpoint analysis, or every 20 min for up to 3 h for kinetic analysis. The NET-DNA release index was reported in comparison with an assigned value of 100% for the total DNA released from cells lysed by 0.5% (*v*/*v*) Triton X-100 as described before with modification (Douda *et al*, 2015; Khan *et al*, 2018). To calculate the kinetic NET-DNA release index in each condition, the fluorescence intensity at time 0 min was subtracted from the fluorescence at each time point and was then divided by the fluorescence values of cell lysed with 0.5% (*v*/*v*) Triton X-100. All the experimental values were standardized to total DNA released by cell lysis. Each condition was tested with a technical triplicate. (iii) For the immunofluorescent imaging quantification analysis of NET formation (Sollberger *et al*, 2016), the equal number of cells was treated by stimuli for 3 h. Then, cell-impermeable DNA dye SYTOX Green (500 nM) was used to detect cells with NET formation, while the total number of cells were determined by staining with cell-permeable DNA dye SYTO Red and phase-contrast imaging. All images were acquired with Fluoview 4.2 software by Olympus confocal microscopy, followed by automated quantification of NETs on 5–6 non-overlapping area per well using ImageJ for quantification of % cells with NET formation.

NET isolation

NETs isolation was processed according to the published literature (Najmeh *et al*, 2015) with modification. Briefly, the conditioned medium of neutrophils with NET formation were gently aspirated and discarded after NETs generation. Cold PBS without Ca^{2+} and Mg^{2+} was used to collect solution of neutrophils with NET formation. All cells were removed by centrifuge at 450 × *g* for 10 min at 4°C; the cell-free NET-rich supernatant was collected and followed by centrifuge at 18,000 × *g* for 10 min at 4°C. The isolated NETs lysed by RIPA lysis buffer containing phosphatase inhibitor cocktail and protease inhibitor cocktail (Roche) and the NET lysates were used for immunoblot assay.

DNA constructs and cell transfection

The pEGFP-C1-lamin B1 was used to generate phosphorylation site mutants. All plasmids for PKCα-consensus phosphorylation site mutant isoforms with single or multiple mutations (pEGFP-C1-lamin B1 S395A, pEGFP-C1-lamin B1 S405A, pEGFP-C1-lamin B1 S408A, pEGFP-C1-lamin B1 S395A/S405A, pEGFP-C1-lamin B1 S395A/S408A, pEGFP-C1-lamin B1 S405A/S408A, pEGFP-C1-lamin B1 S395A/S405A/S408A) were generated as described before (Mall *et al*, 2012). HL-60 (dPMNs) cells were cultured in RPMI-1640 and transfected with HL-60 Cell Avalanche™ (EZ Biosystems) transfection reagent according to the manufacturer's instructions. RAW264.7 cells (ATCC) were cultured in DMEM supplemented with 10% FBS and were transfected with TransIT-Jurket (Mirus) according to the manufacturer's instructions. Forty-eight hours after HL-60 (dPMNs) cell transfection or 24 h after RAW264.7 cell transfection, cells were treated by 10 μM PAF for 3 h and evaluated for induction of extracellular traps, which were then detected as described above.

Confocal fluorescent microscopy analysis

Neutrophils and NETs were fixed with 100% methanol and then stained with primary anti-total PKCα, or anti-phospho-PKCα^{S657}, or anti-lamin B Abs, followed by their matched secondary Abs with FITC or PE conjugation. DNA was stained with DAPI. For measurement of nuclear envelope continuity, the circumferences/perimeters of the cell nucleus, and the lengths of the discontinuity of ruptured nuclear envelope (lamin B staining), of the cells from confocal microscopy images were measured with ImageJ software with modification. Then, the percentages of the discontinuity were calculated according to the above measurements. Confocal fluorescent images were analyzed with an Olympus Fluoview 1000 confocal microscope.

Nuclear protein extraction

To further study the nuclear accumulation of PKCα and its association with nuclear lamin B in neutrophils, the nuclei were extracted using hypotonic buffer according to the published protocol (Shaiken & Opekun, 2014) with modification. In brief, the collected neutrophils were resuspended in ice-cold buffer (pH 7.4) containing 10 mM Tris–HCl, 10 mM NaCl, and 5 mM magnesium acetate for 30 min. NP-40 (0.3%) detergent was then added and homogenized. The mixture homogenates were centrifuged at 1,200 *g* for 10 min at 4°C, to collect sedimented nuclei; these were then resuspended in high volumes of buffer containing 880 mM sucrose and 5 mM magnesium acetate. The suspension was then centrifuged at 2,000 *g* for 20 min at 4°C and nuclei were resuspended in buffer containing 340 mM sucrose and 5 mM magnesium acetate. The recovered nuclei were dissolved in 8 M urea, followed by sonication, and centrifugation by 10,000 *g* for 10 min at 4°C.

Immunoprecipitation (IP)

Immunoprecipation was carried out with direct magnetic IP kit (Pierce) by coupling lamin B antibody (66095-1-Ig, Proteintech) to N-hydroxysuccinimide (NHS)-activated magnetic beads, followed by incubating the lysate with the coupled magnetic beads at 4°C overnight. The immunoprecipitates were then washed twice with cold washing buffer and once with cold ultra-pure water and then bound lamin B was eluted for immunoblot detection of phosphorylated and total lamin B, with anti-p-Ser/Thr/Tyr Ab and anti-lamin B Ab, respectively, in neutrophils that were treated without or with PMA or PAF for 3 h.

Immunoblot analysis

For immunoblot analysis, the cells, that were treated or not, were harvested and washed in ice-cold PBS, and then lysed with RIPA lysis buffer containing phosphatase inhibitor cocktail and protease inhibitor cocktail (Roche). Equal amounts of protein were loaded on SDS–PAGE gel and electrophoresed and then transferred to PVDF membranes. After membrane blocking, they were probed with primary antibodies and matched HRP-conjugated secondary antibodies and then detected using an enhanced chemiluminescent detection kit (Millipore). In some of our immune-blot results, full-length lanes were shown to display the status of lamin B that was

either intact or fragmented. Relative densitometric values of protein bands were quantified by the ImageJ 1.51f software (NIH, USA).

Exposure of mice to ultraviolet B (UVB)

For the experiments with UVB exposure, the dorsal skin was exposed to UVB with two FS40T12-UVB bulbs (LIGHT SOURCES) according to our published protocol (Sharma *et al*, 2011) with modification. Female lamin B transgenic $Lmnb1^{TG}$ mice and their female WT littermates in 8 weeks of age were randomly assigned to receive UVB exposure without/with 150 mJ/cm^2 for five consecutive days under anesthetization by peritoneal injected Ketamine/Xylazine. Animals were sacrificed 24 h after the last exposure. The whole dorsal skin samples, including epidermis, dermis, and subcutaneous fat were collected. Tissue sample sectioning was performed by the Penn Skin Biology and Diseases Resource-based Center.

Fluorescent immunohistochemistry

For immunohistochemistry staining, the paraffin-embedded skin tissue samples were cut into 5 μm sections and placed on glass slides. Slides were placed in a 60°C oven overnight, deparaffinized with CitriSolv (Fisher Scientific) and rehydrated with serial ethanol dilutions. Samples underwent antigen retrieval using Target Retrieval Solutions (DAKO). Peroxidase was deactivated using 0.3% H_2O_2 dissolved in deionized H_2O for 5 min. Sections were blocked using DAKO protein block (Carpintera). The neutrophil markers Ly6G (Amulic *et al*, 2017) and Ly6B (Nakazawa *et al*, 2017) were used for detection of neutrophils as described in other publications in NETosis research. Samples were incubated with primary antibodies overnight at 4°C. Primary antibodies used for staining included Ly6B [Rat anti-neutrophil (7/4), 1:500, Abcam, ab53457], Citrullinated histone H3 (citrulline R2 + R8 + R17) (Rabbit anti-citrullinated Histone H3, 1:300, Abcam, ab5103), IL-17A (Rabbit anti-IL-17A, 1:100, Abcam, ab79056). Goat anti-rat IgG secondary antibody conjugated with Alexa Fluor® 647 (1:500, Invitrogen) and donkey anti-rabbit IgG secondary antibody conjugated with Alexa Fluor®488 (1:500, Invitrogen) were used to detect primary antibodies. In separate experiments, PE-conjugated rat anti-mouse Ly6G antibody (BioLegend) was used for neutrophil detection. FITC anti-mouse TNFα antibody (Rat anti-TNFα, 1:100, BioLegend, 506304) was also used for immunofluorescent staining. Isotype-matched IgG was used instead of primary antibody as a negative control of the staining. Counterstaining with DAPI was performed and slides were mounted with SlowFade Gold Antifade Mountant (Invitrogen). Images were obtained using the Nikon Eclipse fluorescent microscope, and the fluorescent staining area percentage was analyzed by Nikon NIS-Elements Advanced Research software, according to previous publication (Brinkmann *et al*, 2016).

Quantification and statistical analysis

Prism 6 (GraphPad Software) was used to perform statistical analysis. Normally distributed data are shown as means ± standard deviations (SD). Comparisons between two groups were conducted with the Student *t* test. Comparisons among three or more groups were performed using ANOVA, followed by Student–Newman–Keuls test. Statistical significance was considered at a level of P-value < 0.05.

Data availability

No primary datasets have been generated and deposited.

Expanded View for this article is available online.

Acknowledgements
The authors would like to acknowledge Penn Skin Biology and Diseases Resource-based Center for their skin histology service. The authors would like to thank Debra A. Pawlowski (animal facility, Philadelphia VA Medical Center) for her kindly help with our animal experiments. The authors would also thank Dr. Iain W. Mattaj for his support on the lamin B mutation work. This work was supported by Lupus Research Alliance (416805) and NIH R21AI144838 (to MLL), and the Veterans Affairs Merit Review Award (to VPW), ERC StG No 804710 and the Hector Stiftung II gGmbH (to MM), and a Helmholtz International Graduate School Fellowship (BW).

Author contributions
M-LL conceived and designed the study. YL, ML, M-LL performed the laboratory experiments and analyzed the experimental data. For the confocal image analysis, M-LL took the images, and YL and MHL conducted further quantification and statistical analysis. MM and BW made the plasmids for the lamin B mutations. M-LL, YL, VPW, MM wrote/drafted and finalized the paper. All authors read and approved the final manuscript.

Conflict of interest
The authors declare that they have no conflict of interest.

References

Adam SA, Butin-Israeli V, Cleland MM, Shimi T, Goldman RD (2013) Disruption of lamin B1 and lamin B2 processing and localization by farnesyltransferase inhibitors. *Nucleus* 4: 142 – 150

Amulic B, Knackstedt SL, Abu Abed U, Deigendesch N, Harbort CJ, Caffrey BE, Brinkmann V, Heppner FL, Hinds PW, Zychlinsky A (2017) Cell-cycle proteins control production of neutrophil extracellular traps. *Dev Cell* 43: 449 – 462

Arroyo A, Modrianský M, Serinkan FB, Bello RI, Matsura T, Jiang J, Tyurin VA, Tyurina YY, Fadeel B, Kagan VE (2002) NADPH oxidase-dependent oxidation and externalization of phosphatidylserine during apoptosis in Me2SO-differentiated HL-60 cells. Role in phagocytic clearance. *J Biol Chem* 277: 49965 – 49975

Azzouz D, Khan MA, Sweezey N, Palaniyar N (2018) Two-in-one: UV radiation simultaneously induces apoptosis and NETosis. *Cell Death Discov* 4: 51

Bashir MM, Sharma MR, Werth VP (2009) UVB and proinflammatory cytokines synergistically activate TNF-alpha production in keratinocytes through enhanced gene transcription. *J Invest Dermatol* 129: 994 – 1001

Boeltz S, Amini P, Anders HJ, Andrade F, Bilyy R, Chatfield S, Cichon I, Clancy DM, Desai J, Dumych T *et al* (2019) To NET or not to NET:current opinions and state of the science regarding the formation of neutrophil extracellular traps. *Cell Death Differ* 26: 395 – 408

Bornancin F, Parker PJ (1997) Phosphorylation of protein kinase C-alpha on serine 657 controls the accumulation of active enzyme and contributes to its phosphatase-resistant state. *J Biol Chem* 272: 3544 – 3549

Boxio R, Bossenmeyer-Pourie C, Steinckwich N, Dournon C, Nube O (2004) Mouse bone marrow contains large numbers of functionally competent neutrophils. *J Leukoc Biol* 75: 604 – 611

Braz JC, Gregory K, Pathak A, Zhao W, Sahin B, Klevitsky R, Kimball TF, Lorenz JN, Nairn AC, Liggett SB *et al* (2004) PKC-alpha regulates cardiac contractility and propensity toward heart failure. *Nat Med* 10: 248 – 254

Brinkmann V, Reichard U, Goosmann C, Fauler B, Uhlemann Y, Weiss DS, Weinrauch Y, Zychlinsky A (2004) Neutrophil extracellular traps kill bacteria. *Science* 303: 1532 – 1535

Brinkmann V, Abu Abed U, Goosmann C, Zychlinsky A (2016) Immunodetection of NETs in paraffin-embedded tissue. *Front Immunol* 7: 513

Chen KW, Monteleone M, Boucher D, Sollberger G, Ramnath D, Condon ND, von Pein JB, Broz P, Sweet MJ, Schroder K (2018) Noncanonical inflammasome signaling elicits gasdermin D-dependent neutrophil extracellular traps. *Sci Immunol* 3: eaar6676

Collas P, Thompson L, Fields AP, Poccia DL, Courvalin JC (1997) Protein kinase C-mediated interphase lamin B phosphorylation and solubilization. *J Biol Chem* 272: 21274 – 21280

Damiani E, Ullrich SE (2016) Understanding the connection between platelet-activating factor, a UV-induced lipid mediator of inflammation, immune suppression and skin cancer. *Prog Lipid Res* 63: 14 – 27

Denny MF, Yalavarthi S, Zhao W, Thacker SG, Anderson M, Sandy AR, McCune WJ, Kaplan MJ (2010) A distinct subset of proinflammatory neutrophils isolated from patients with systemic lupus erythematosus induces vascular damage and synthesizes type I IFNs. *J Immunol* 184: 3284 – 3297

Douda DN, Khan MA, Grasemann H, Palaniyar N (2015) SK3 channel and mitochondrial ROS mediate NADPH oxidase-independent NETosis induced by calcium influx. *Proc Natl Acad Sci USA* 112: 2817 – 2822

Etulain J, Martinod K, Wong SL, Cifuni SM, Schattner M, Wagner DD (2015) P-selectin promotes neutrophil extracellular trap formation in mice. *Blood* 126: 242 – 246

Folkesson M, Li C, Frebelius S, Swedenborg J, Wagsater D, Williams KJ, Eriksson P, Roy J, Liu ML (2015) Proteolytically active ADAM10 and ADAM17 carried on membrane microvesicles in human abdominal aortic aneurysms. *Thromb Haemost* 114: 1165 – 1174

Fontayne A, Dang P, Gougerot-Pocidalo M, El Benna J (2001) Phosphorylation of $p47^{phox}$ sites by PKC α, βII, δ, and ζ: effect on binding to $p22^{phox}$ and on NADPH oxidase activation. *Biochemistry* 41: 7743 – 7750

Fuchs TA, Abed U, Goosmann C, Hurwitz R, Schulze I, Wahn V, Weinrauch Y, Brinkmann V, Zychlinsky A (2007) Novel cell death program leads to neutrophil extracellular traps. *J Cell Biol* 176: 231 – 241

Giambelluca MS, Bertheau-Mailhot G, Laflamme C, Rollet-Labelle E, Servant MJ, Pouliot M (2014) TNF-alpha expression in neutrophils and its regulation by glycogen synthase kinase-3: a potentiating role for lithium. *FASEB J* 28: 3679 – 3690

Goldberg MW, Huttenlauch I, Hutchison CJ, Stick R (2008) Filaments made from A- and B-type lamins differ in structure and organization. *J Cell Sci* 121: 215 – 225

Griffin GK, Newton G, Tarrio ML, Bu DX, Maganto-Garcia E, Azcutia V, Alcaide P, Grabie N, Luscinskas FW, Croce KJ *et al* (2012) IL-17 and TNF-alpha sustain neutrophil recruitment during inflammation through synergistic effects on endothelial activation. *J Immunol* 188: 6287 – 6299

Hamam H, Khan M, Palaniyar N (2019) Histone acetylation promotes neutrophil extracellular trap formation. *Biomolecules* 9: 32

Hatch E, Hetzer M (2014) Breaching the nuclear envelope in development and disease. *J Cell Biol* 205: 133 – 141

Heng MY, Lin ST, Verret L, Huang Y, Kamiya S, Padiath QS, Tong Y, Palop JJ, Huang EJ, Ptacek LJ *et al* (2013) Lamin B1 mediates cell-autonomous neuropathology in a leukodystrophy mouse model. *J Clin Investig* 123: 2719 – 2729

Hocevar BA, Burns DJ, Fields AP (1993) Identification of protein kinase C (PKC) phosphorylation sites on human lamin B. Potential role of PKC in nuclear lamina structural dynamics. *J Biol Chem* 268: 7545 – 7552

Justus CR, Leffler N, Ruiz-Echevarria M, Yang LV (2014) *In vitro* cell migration and invasion assays. *J Vis Exp*: 51046

Khan MA, Philip LM, Cheung G, Vadakepeedika S, Grasemann H, Sweezey N, Palaniyar N (2018) Regulating NETosis: increasing pH promotes NADPH oxidase-dependent NETosis. *Front Med* 5: 19

Konig MF, Andrade F (2016) A critical reappraisal of neutrophil extracellular traps and NETosis mimics based on differential requirements for protein citrullination. *Front Immunol* 7: 461

Lammerding J, Fong LG, Ji JY, Reue K, Stewart CL, Young SG, Lee RT (2006) Lamins A and C but not lamin B1 regulate nuclear mechanics. *J Biol Chem* 281: 25768 – 25780

Li H, Prasad R, Katiyar SK, Yusuf N, Elmets CA, Xu H (2015) Interleukin-17 mediated inflammatory responses are required for ultraviolet radiation-induced immune suppression. *Photochem Photobiol* 91: 235 – 241

Lin AM, Rubin CJ, Khandpur R, Wang JY, Riblett M, Yalavarthi S, Villanueva EC, Shah P, Kaplan MJ, Bruce AT (2011) Mast cells and neutrophils release IL-17 through extracellular trap formation in psoriasis. *J Immunol* 187: 490 – 500

Liu Y, Mei J, Gonzales L, Yang G, Dai N, Wang P, Zhang P, Favara M, Malcolm KC, Guttentag S *et al* (2011) IL-17A and TNF-alpha exert synergistic effects on expression of CXCL5 by alveolar type II cells *in vivo* and *in vitro*. *J Immunol* 186: 3197 – 3205

Lood C, Blanco LP, Purmalek MM, Carmona-Rivera C, De Ravin SS, Smith CK, Malech HL, Ledbetter JA, Elkon KB, Kaplan MJ (2016) Neutrophil extracellular traps enriched in oxidized mitochondrial DNA are interferogenic and contribute to lupus-like disease. *Nat Med* 22: 146 – 153

Machowska M, Piekarowicz K, Rzepecki R (2015) Regulation of lamin properties and functions: does phosphorylation do it all? *Open Biol* 5: 150094

Mall M, Walter T, Gorjanacz M, Davidson IF, Nga Ly-Hartig TB, Ellenberg J, Mattaj IW (2012) Mitotic lamin disassembly is triggered by lipid-mediated signaling. *J Cell Biol* 198: 981 – 990

Martelli AM, Evangelisti C, Nyakern M, Manzoli FA (2006) Nuclear protein kinase C. *Biochem Biophys Acta* 1761: 542 – 551

Martinod K, Witsch T, Farley K, Gallant M, Remold-O'Donnell E, Wagner DD (2016) Neutrophil elastase-deficient mice form neutrophil extracellular traps in an experimental model of deep vein thrombosis. *J Thromb Haemost* 14: 551 – 558

Moisan E, Girard D (2006) Cell surface expression of intermediate filament proteins vimentin and lamin B1 in human neutrophil spontaneous apoptosis. *J Leukoc Biol* 79: 489 – 498

Muranyi W, Haas J, Wagner M, Krohne G, Koszinowski UH (2002) Cytomegalovirus recruitment of cellular kinases to dissolve the nuclear lamina. *Science* 297: 854 – 857

Najmeh S, Cools-Lartigue J, Giannias B, Spicer J, Ferri LE (2015) Simplified human neutrophil extracellular traps (NETs) isolation and handling. *J Vis Exp*: 52687

Nakazawa D, Kumar SV, Marschner J, Desai J, Holderied A, Rath L, Kraft F, Lei Y, Fukasawa Y, Moeckel GW *et al* (2017) Histones and neutrophil extracellular traps enhance tubular necrosis and remote organ injury in ischemic AKI. *J Am Soc Nephrol* 28: 1753 – 1768

Neeli I, Khan SN, Radic M (2008) Histone deimination as a response to inflammatory stimuli in neutrophils. *J Immunol* 180: 1895 – 1902

Neri LM, Borgatti P, Capitani S, Martelli AM (1998) Nuclear diacylglycerol produced by phosphoinositide-specific phospholipase C is responsible for nuclear translocation of protein kinase C-alpha. *J Biol Chem* 273: 29738 – 29744

Neubert E, Meyer D, Rocca F, Gunay G, Kwaczala-Tessmann A, Grandke J, Senger-Sander S, Geisler C, Egner A, Schon MP *et al* (2018) Chromatin swelling drives neutrophil extracellular trap release. *Nat Commun* 9: 3767

Neubert E, Bach KM, Busse J, Bogeski I, Schon MP, Kruss S, Erpenbeck L (2019) Blue and long-wave ultraviolet light induce *in vitro* neutrophil extracellular trap (NET) formation. *Front Immunol* 10: 2428

Olins AL, Zwerger M, Herrmann H, Zentgraf H, Simon AJ, Monestier M, Olins DE (2008) The human granulocyte nucleus: unusual nuclear envelope and heterochromatin composition. *Eur J Cell Biol* 87: 279 – 290

Papayannopoulos V, Metzler KD, Hakkim A, Zychlinsky A (2010) Neutrophil elastase and myeloperoxidase regulate the formation of neutrophil extracellular traps. *J Cell Biol* 191: 677 – 691

Park R, Baines JD (2006) Herpes simplex virus type 1 infection induces activation and recruitment of protein kinase C to the nuclear membrane and increased phosphorylation of lamin B. *J Virol* 80: 494 – 504

Pieterse E, Rother N, Yanginlar C, Gerretsen J, Boeltz S, Munoz LE, Herrmann M, Pickkers P, Hilbrands LB, van der Vlag J (2018) Cleaved N-terminal histone tails distinguish between NADPH oxidase (NOX)-dependent and NOX-independent pathways of neutrophil extracellular trap formation. *Ann Rheum Dis* 77: 1790 – 1798

Pilsczek FH, Salina D, Poon KK, Fahey C, Yipp BG, Sibley CD, Robbins SM, Green FH, Surette MG, Sugai M *et al* (2010) A novel mechanism of rapid nuclear neutrophil extracellular trap formation in response to *Staphylococcus aureus*. *J Immunol* 185: 7413 – 7425

Remijsen Q, Vanden Berghe T, Wirawan E, Asselbergh B, Parthoens E, De Rycke R, Noppen S, Delforge M, Willems J, Vandenabeele P (2011) Neutrophil extracellular trap cell death requires both autophagy and superoxide generation. *Cell Res* 21: 290 – 304

Rochael NC, Guimaraes-Costa AB, Nascimento MT, DeSouza-Vieira TS, Oliveira MP, GarciaeSouza LF, Oliveira MF, Saraiva EM (2015) Classical ROS-dependent and early/rapid ROS-independent release of Neutrophil Extracellular Traps triggered by Leishmania parasites. *Sci Rep* 5: 18302

Rowat AC, Jaalouk DE, Zwerger M, Ung WL, Eydelnant IA, Olins DE, Olins AL, Herrmann H, Weitz DA, Lammerding J (2013) Nuclear envelope composition determines the ability of neutrophil-type cells to passage through micron-scale constrictions. *J Biol Chem* 288: 8610 – 8618

Ruddy MJ, Wong GC, Liu XK, Yamamoto H, Kasayama S, Kirkwood KL, Gaffen SL (2004) Functional cooperation between interleukin-17 and tumor necrosis factor-alpha is mediated by CCAAT/enhancer-binding protein family members. *J Biol Chem* 279: 2559 – 2567

Shaiken TE, Opekun AR (2014) Dissecting the cell to nucleus, perinucleus and cytosol. *Sci Rep* 4: 4923

Sharma MR, Werth B, Werth VP (2011) Animal models of acute photodamage: comparisons of anatomic, cellular and molecular responses in C57BL/6J, SKH1 and Balb/c mice. *Photochem Photobiol* 87: 690 – 698

Shimizu T, Cao CX, Shao RG, Pommier Y (1998) Lamin B phosphorylation by protein kinase calpha and proteolysis during apoptosis in human leukemia HL60 cells. *J Biol Chem* 273: 8669 – 8674

Shin JW, Spinler KR, Swift J, Chasis JA, Mohandas N, Discher DE (2013) Lamins regulate cell trafficking and lineage maturation of adult human hematopoietic cells. *Proc Natl Acad Sci USA* 110: 18892 – 18897

Singh N, Johnstone DB, Martin KA, Tempera I, Kaplan MJ, Denny MF (2016) Alterations in nuclear structure promote lupus autoimmunity in a mouse model. *Dis Models Mech* 9: 885 – 897

Slee EA, Adrain C, Martin SJ (2001) Executioner caspase-3, -6, and -7 perform distinct, non-redundant roles during the demolition phase of apoptosis. *J Biol Chem* 276: 7320 – 7326

Soehnlein O, Steffens S, Hidalgo A, Weber C (2017) Neutrophils as protagonists and targets in chronic inflammation. *Nat Rev Immunol* 17: 248 – 261

Sollberger G, Amulic B, Zychlinsky A (2016) Neutrophil extracellular trap formation is independent of *de novo* gene expression. *PLoS One* 11: e0157454

Sollberger G, Choidas A, Burn GL, Habenberger P, Di Lucrezia R, Kordes S, Menninger S, Eickhoff J, Nussbaumer P, Klebl B *et al* (2018) Gasdermin D plays a vital role in the generation of neutrophil extracellular traps. *Sci Immunol* 3: eaar6689

Swift J, Ivanovska IL, Buxboim A, Harada T, Dingal PC, Pinter J, Pajerowski JD, Spinler KR, Shin JW, Tewari M *et al* (2013) Nuclear lamin-A scales with tissue stiffness and enhances matrix-directed differentiation. *Science* 341: 1240104

Tatsiy O, McDonald PP (2018) Physiological stimuli induce PAD4-dependent, ROS-independent NETosis, with early and late events controlled by discrete signaling pathways. *Front Immunol* 9: 2036

Vergnes L, Peterfy M, Bergo MO, Young SG, Reue K (2004) Lamin B1 is required for mouse development and nuclear integrity. *Proc Natl Acad Sci USA* 101: 10428 – 10433

Wang Y, Li M, Stadler S, Correll S, Li P, Wang D, Hayama R, Leonelli L, Han H, Grigoryev SA *et al* (2009) Histone hypercitrullination mediates chromatin decondensation and neutrophil extracellular trap formation. *J Cell Biol* 184: 205 – 213

Yipp BG, Kubes P (2013) NETosis: how vital is it? *Blood* 122: 2784 – 2794

Zawrotniak M, Bartnicka D, Rapala-Kozik M (2019) UVA and UVB radiation induce the formation of neutrophil extracellular traps by human polymorphonuclear cells. *J Photochem Photobiol B* 196: 111511

